The Amplitude and Timescales of 0-15 ka Paleomagnetic Secular Variation in the Northern North Atlantic

Brendan T. Reilly[1], Joseph S. Stoner[2], Sædís Ólafsdóttir[3], Anne Jennings[4], Robert Hatfield[5], Gréta Björk Kristjánsdóttir[6], Áslaug Geirsdóttir[7]

[1]Lamont-Doherty Earth Observatory, Columbia University, Palisades, NY 10964, USA

[2]College of Earth, Ocean, and Atmospheric Sciences, Oregon State University, Corvallis, OR 97331, USA

[3]Reykjavík Energy, Reykjavík, Iceland

[4]INSTAAR, University of Colorado, Boulder, CO 80309, USA

[5]Department of Geological Sciences, University of Florida, Gainesville, FL 32611, USA

[6]School of Engineering and Natural Sciences, University of Iceland, Reykjavík, Iceland

[7]Faculty of Earth Sciences, University of Iceland, Reykjavík, Iceland

Corresponding author: Brendan T. Reilly, breilly@ldeo.columbia.edu

Key Points:

- Sediment cores with ultra-high accumulation rates are used to study directional changes in the Northern North Atlantic's geomagnetic field
- Study addresses uncertainties in sedimentary paleomagnetic research, such as signal attenuation, chronology, and reproducibility
- Study reveals robust variability on centennial timescales with greater variance than generally observed over the last 15,000 years

Abstract

We investigate the amplitude and frequency of directional geomagnetic change since 15 ka in the Northern North Atlantic (~67° N) using 5 'ultra-high' resolution continental shelf sediment cores deposited at rates greater than 1 m/kyr. The ages of these cores are constrained by 103 radiocarbon dates with reservoir ages assessed through tephra correlation to terrestrial archives. Our study aims to address many of the uncertainties that are common in sedimentary paleomagnetic studies, including signal attenuation in low to moderate resolution archives and difficulty to demonstrate reproducibility in higher resolution archives. The 'ultra-high' accumulation rates of our cores reduce 'lock-in' and smoothing uncertainties associated with magnetic acquisition processes. Abundant radiocarbon dates along with an objective alignment algorithm provide a test of signal reproducibility at sub-millennial timescales. The PSV signal, evaluated as individual records and as a new stack (GREENICE15k), validates prior results, but provides stronger geochronological constraints, demonstrates a reproducible PSV signal and amplitude, and extends through the abrupt Bølling–Allerød and Younger Dryas climate transitions of the latest Pleistocene. While broadly consistent with time-varying spherical harmonic models and varve dated records from Northern Europe, we demonstrate greater variance and higher amplitudes—particularly at sub-millennial timescales. This robust variability on centennial timescales is rarely observed or discussed, but is likely important to our understanding of some of the most intriguing aspects of the geodynamo.

Plain Language Summary

Our study used mud from the seafloor to investigate changes in Earth's magnetic field in the Northern North Atlantic region over the past 15 thousand years. Magnetic minerals eroded from rocks and deposited on the seafloor can preserve a record of the geomagnetic field, like little compass needles suspended in mud. We obtained sediment cores from areas near land with very high accumulation rates, which are rare in the modern ocean, that can record short magnetic field variations that occur on the timescale of centuries. We used radiocarbon dating to determine the ages of the sediment samples and a new alignment algorithm to verify the accuracy and consistency of the magnetic signal we observed. Understanding these short geomagnetic field variations is challenging, but it is key to unlocking many mysteries about the past and future of Earth's magnetic field.

1. Introduction

Reconstructing the ancient magnetic field is not a trivial task and many mysteries remain. Yet, recent improvements in paleomagnetic field modeling demonstrate a dynamic and complex field (e.g., Constable et al., 2016; Nilsson et al., 2022; Panovska et al., 2021, 2019) with the largest uncertainties typically stemming from data quality, geochronology, and spatiotemporal coverage. To improve our understanding of what components are missing in our field reconstructions, we explore the first two of these issues in the directional record of sedimentary archives—posing the questions, *what are the full amplitude and frequency characteristics of geomagnetic change? And do sediments ever capture them?*

Sediment paleomagnetic archives are globally distributed, continuous, and can be well dated. However, even if sediments are perfectly recovered with no disturbance, they can also be complicated by environmentally driven lithologic variability, variable accumulation rates, and smoothing/offsets associated with post-depositional remanent magnetization (pDRM) acquisition and sampling/measurement methods. Sediment deposits with accumulation high enough to minimize the effects of pDRM are rare, often have complex lithologies, and can be difficult to reproduce on regional scales without supervised correlation. Yet, in rare circumstances high deposition rate environments with intervals of generally homogenous lithologies are clustered, allowing us to circumvent these issues. In this study we leverage a collection of sedimentary paleomagnetic secular variation (PSV) records from continental shelves ~67° N in the Northern North Atlantic (**Figure 1**) that target deposits with abundant radiocarbon dates and accumulation rates greater than 100 cm/kyr.

Based on the reasonable assumption that sediments within a limited geographic region have experienced a common geomagnetic history (see Korte et al., 2019), we begin by using the PSV records to align stratigraphies irrespective of age using an objective alignment algorithm (Hagen et al., 2020). These depth-to-depth correlations, which we call geomagnetic network analysis (GNA), allow regional organization of each stratigraphy's chronologic constraints (in this case, radiocarbon dates and tephra horizons) from multiple sequences to be combined into a single age-depth profile (c.f., Reilly et al., 2018; Stoner et al., 2007). The caveats of GNA are: 1) that the region must be small enough that the records under consideration were influenced by a common geomagnetic field through time, and 2) that the field was faithfully recorded at or near the time of deposition in a generally unaltered state at each site (essentially the same for any paleo-geomagnetic record). By using stratigraphic sequences from different depositional environments, we reduce the potential for systematic errors and provide a check for geologic uncertainties that can often go undetected. Similarly, by organizing the records and

stratigraphic information on a regional correlated equivalent depth scale, chronology can be easily updated with future radiocarbon calibration curves and improved understanding of the time variations in radiocarbon reservoir effects.

2. Materials and Methods

We organize previously published and new paleomagnetic and stratigraphic data from high accumulation rate depocenters on the North Iceland and Southeast Greenland Shelf collected from the Marion Dufresne II as part of the 1999 IMAGES-V campaign with the long Calypso Corer (**Figure 1**). Radiocarbon data are organized in **Supplemental Tables S1 and S2**, tephra data are organized in **Supplemental Table S3**, and paleomagnetic data are archived in the MagIC and Zenodo databases. All natural remanent magnetization (NRM) data were collected on u-channel samples at the University of California Davis paleomagnetic laboratory using a 2G Enterprises™ Model 755 cryogenic magnetometer, before and after progressive alternating field demagnetization (see Stoner et al., 2007). While measurements were made every 1 cm, the response function of the magnetometer integrates the magnetization over a ~4.5 cm interval. Although discrete samples may provide an advantage in many depositional environments with lower accumulation rates to obtain higher temporal resolution and deal with complex variations in magnetic remanence carriers (e.g., Nowaczyk et al., 2021), for this study, this response function only smooths the paleomagnetic signal on decadal timescales at most, as we only focus on sediments deposited at rates greater than 100 cm/kyr.

Paleomagnetic data from cores MD99-2269 and MD99-2322 are previously published and we use those data as reported in their original publication (Stoner et al., 2007). Data from MD99-2264, MD99-2265, and MD99-2266 were checked and corrected for flux jumps using UPMAG and UDECON MATLAB tools (Xuan and Channell, 2009; Xuan and Oda, 2015). Flux jumps can be difficult to predict, but are most commonly observed when the rate of flux change is too great (Bowles, 2009). However, in some cases, these flux jumps appear to be random and are characterized by an abrupt change in the flux counts on a particular axis. These types of flux jumps can be observed in continuous u-channel data, but are often obscured and overlooked by automatic drift correction (Oda and Shibuya, 1996; Xuan and Channell, 2009). The UPMAG analysis identified common, but previously unrecognized, flux jumps on the X-axis on the UC Davis system when Cores MD99-2265 and MD99-2266 were run in Fall 1999 that added artifacts to the original data (**Supplemental Figures S1 and S2**). The UPMAG UCHECK algorithm effectively

corrected for this issue, as discussed below. MD99-2264 was measured in Spring 2005 and flux jumps were not observed in those data.

Hysteresis loops and backfield curves were measured on bulk sediments sampled from cores MD99-2269 and MD99-2322 at a nominal 500-year resolution. Saturation magnetization (M_s), Remanent Magnetization (M_r) and Bulk Coercivity (H_c) was derived from the hysteresis loops using a saturating field of 1,000 mT following correction for the paramagnetic slope above 800 mT. The coercivity of remanence (H_{cr}) was determined by demagnetization of the 1,000 mT M_r in 2.5 mT steps. All measurements were made on a Princeton Measurements Corporation Micromag model 3900 vibrating sample magnetometer (VSM) at Western Washington University.

2.1 MD99-2264

Core MD99-2264 is located in the Djúpáll trough on the Northwest Iceland Shelf (66.68^o N, 24.20^o W; 235 m water depth). The core is 37.79 m long and contains deglacial to Holocene aged sediments. The base of the core is a stiff, massive diamict, overlain by fining up sequences of sand, silt and clay, indicating deposition at or near the marine terminating Iceland Ice Cap margin (Geirsdóttir et al., 2002). Above these sediments is a more distal silty clay and sandy silt glaciomarine facies with ice rafted debris (IRD) which eventually transitions into post glacial massive fine-grained sand with abundant shells (Geirsdóttir et al., 2002). 24 radiocarbon dates were previously published by Geirsdóttir et al. (2002) and Ólafsdóttir et al. (2010), although the radiocarbon dates below 30 m likely indicate reworking. Our age model only uses the 19 dates used by Ólafsdóttir et al. (2010) and indicate the upper 27.5 m span the last ~15 kyrs, with high accumulation rates suitable for our study from ~9-15 ka. Two visible ashes, the Saksunarvatn ash found at 5 m and the Vedde ash found at 11.83 m, were reported (Geirsdóttir et al., 2002). Paleomagnetic data for MD99-2264 has not been published previously; however, the data were previously discussed in the Ph.D. thesis of Ólafsdóttir (2010).

2.2 MD99-2265

Core MD99-2265 was recovered from Jökulfirðir, a tributary fjord system of Ísafjarðardjúp in the Vestfirðir region of Iceland in a basin formed between two submarine moraine ridges (66.28^o N, 22.86^o W; 93 m water depth). The core is just over 17 m long and lithology is primarily silty clay, with IRD present near the base of the core, below ~10 m (Geirsdóttir et al., 2002). 14 radiocarbon dates have

been reported by Geirsdóttir et al. (2002) and indicate that MD99-2265 spans the last ~13 kyr, with suitable accumulation rates for our study between ~7 and 12 ka. The Saksunarvatn ash was identified at 10.69 m (Geirsdóttir et al., 2002). Paleomagnetic data for MD99-2265 has not been published previously; however, the uncorrected data with flux jumps on the X-axis was previously discussed in the Ph.D. thesis of Ólafsdóttir (2010).

2.3 MD99-2266

Core MD99-2266 was recovered from near the mouth of Ísafjarðardjúp, in the Vestfirðir region of Iceland behind a shallow-water sill (66.23° N, 23.27° W; 106 m water depth). This core is 38.9 m in length and has 24 published radiocarbon dates, spanning the last ~11 kyr with high enough accumulation rates for this study spanning almost that entire interval (Andrews et al., 2008; Quillmann et al., 2010). The Saksunarvatn ash was identified at 35.91 m (Quillmann et al., 2010). Declination and inclination were previously published by Andrews et al. (2008) with broad similarities in inclination noted when compared with MD99-2269, previously published by Stoner et al. (2007). However, much of the noise in MD99-2266 noted by Andrews et al. (2008) can be attributed to the previously mentioned undetected flux jumps on the X-axis. The Xuan and Channell (2009) UPMAG corrected data presented here are a significant improvement with lower maximum angular deviation (MAD; Kirschvink, 1980) values and better agreement with other records, as documented later in this study and in **Supplementary Figure 2**.

2.4 MD99-2269

Core MD99-2269 was recovered from Húnaflóadjúp on the North Iceland Shelf (66.63° N, 20.85° W; 365 m water depth). The core is 25.33 m in length with 27 published radiocarbon dates, spanning ~12 kyr with accumulation rates that vary between ~300-400 cm/kyr from 9.5-12 ka and ~100-300 cm/kyr after 9.5 ka (Stoner et al., 2007). Detailed tephra and cryptotephra analysis has identified numerous ash layers, including the Saksunarvatn ash (Kristjánsdóttir et al., 2007), which, through correlation to equivalent tephra in terrestrial sequences, has been used to assess radiocarbon reservoir ages (Stoner et al., 2013). The core has received considerable attention for paleoenvironmental and paleoclimate purposes, thanks to its strong age model and high accumulation rates (Andrews et al., 2003; Cabedo-Sanz et al., 2016; Geirsdóttir et al., 2020; Kristjánsdóttir et al., 2017). The paleomagnetic data were

originally published and discussed by Stoner et al. (2007), who noted a high resolution, high amplitude, and regionally reproducible signal that has since been further documented as a robust signal (Hagen et al., 2020; Stoner et al., 2013; Walczak et al., 2017), been used as a template to assess or constrain regional records (Caron et al., 2019; Korte et al., 2019; Ólafsdóttir et al., 2019, 2013; Reilly et al., 2019; Strunk et al., 2018), and is an important record for Holocene field modeling (Nilsson et al., 2022). It is one of the two records, with MD99-2322, used to create the Greenland/Iceland PSV stack of Stoner et al. (2013).

2.5 MD99-2322

Core MD99-2322 was recovered from the deepest part of the Kangerlussuaq Trough (67.14° N, 30.83° W; 714 m water depth). The core is 26.17 m in length with 20 published radiocarbon dates, with ~300-600 cm/kyr accumulation rate from 9-12 ka and ~100-200 cm/kyr accumulation rates after (Stoner et al., 2007). Detailed tephra and cryptotephra analysis has identified many tephra, but none are definitively correlative to those found in the four North Iceland cores used in this study (Jennings et al., 2014). The paleomagnetic data were first published and discussed by Stoner et al. (2007) and, like MD99-2269, has been studied in subsequent work and demonstrated to be a high resolution and reproducible signal (Hagen et al., 2020; Stoner et al., 2013).

3. Results

3.1 Paleomagnetism and Rock Magnetism

Like previously documented (e.g., Stoner et al., 2007), cores from this region often have well defined Characteristic Remanent Magnetizations (ChRM) that have low MAD values with single component magnetizations that trend towards the origin on an orthogonal projection plot (**Figure 2; Supplementary Figure S1**). ChRMs were isolated using a principle component analysis over a range of AF demagnetization steps. The same demagnetization steps were used for all the horizons in each core, but varied between cores depending on which measurements were made and what range best isolated the ChRM for Cores 2264 (20, 30, 40, 50, and 60 mT peak AF), 2265 (10, 20, 30, 40, 50, and 60 mT peak AF), 2266 (10, 20, 25, 30, 35, 40, and 50 mT peak AF), 2269 (10, 20, 30, 40, 50, and 60 mT peak AF), and

2322 (10, 20 25, 30, 35, 40, 50, 60 mT peak AF). Nearly all resulting MAD values for the 5 cores reported here are less than 5° (**Figure 2**).

For Cores 2265, and 2266, the data presented here differ from those initially presented in the Ph.D. thesis of Ólafsdóttir (2010) and by Andrews et al. (2008), due to the previously mentioned flux jumps that appear to have been common on the X-axis of the UC Davis magnetometer when these cores were run in Fall 1999. These flux jumps were detected and corrected using the algorithms in UPMAG and UDECON MATLAB tools (Xuan and Channell, 2009; Xuan and Oda, 2015). We are confident that these flux jump corrections improve the data, as it decreases the number of abrupt changes in downcore declination changes, and it improves the agreement between demagnetization steps (**Supplementary Figure S1A**). The latter of these points is especially important, as the flux jump corrections for each demagnetization step was processed separately and the improvement can be seen in more systematic demagnetization to the origin on orthogonal demagnetization plots and resulting decrease in MAD values (**Supplementary Figure S1B**). Previously, the original data for Core 2266 were published by Andrews et al. (2008) and, while having many similarities to the long-period signal documented in Core 2269, showed many additional high amplitude features in inclination and declination and high MAD values. The flux jump corrections we apply in this study remove many of these spurious inclination and declination features, significantly lowered MAD values, and, as we discuss later in this study, significantly improve regional correlation with other PSV records (**Supplementary Figure S2**).

High mass normalized M_s values for Cores MD99 2269 and 2322 (median values 0.75 and 0.83 Am^2/kg, respectively) suggest high concentration of ferrimagnetic minerals (**Figure 3A**). Within each core, hysteresis loops are relatively uniform, indicating both homogeneity and downcore stability in the magnetic mineral assemblage. All hysteresis loops acquire 95 – 97 % of their M_s value in a field of 300 mT, consistent with (titano)magnetite being the dominant remanence carrying mineral (**Figure 3B**). In Day Plot space (Day et al., 1977), samples from both cores cluster tightly and fall within the M_{rs}/M_s range of terrestrial clays, silts, and sands from Greenland and Iceland and the range of previously published sediment cores from the Iceland and Greenland margins (**Figure 3C**). Slightly lower M_{rs}/M_s values in Core 2322 occur during the early Holocene and their timing likely reflects increased input of terrestrial silt-sized sediments from Greenland (**Figure 3C**; Hatfield et al., 2017) rather than the effect of significant sediment diagenesis, which from the rock magnetic data appears to be minor.

3.2 Age Model and Reservoir Ages

One of the major challenges in radiocarbon age modeling is determining a suitable reservoir correction to account for the fact that the ocean has a spatially and temporally variable reservoir of old carbon, relative to atmospheric radiocarbon contents. The Marine20 calibration curve accounts for this reservoir effect through the use of a carbon cycle model to develop global scale marine reservoir age (MRA) (Heaton et al., 2020). A parameter called ΔR is used at the site level to account for regional water mass deviations from the global MRA (Stuiver et al., 1986). It is important to note that the Marine20 MRA correction is different than previous marine radiocarbon calibration curves, with Marine20 attempting to take most large scale MRA effects into account (Heaton et al., 2022). The result is an offset from atmospheric calibration that is on average ~150 years greater than Marine13 during the Holocene (Heaton et al., 2020; Reimer et al., 2013) (**Supplemental Figure S3**). However, we note that this is not a constant offset and Marine20 implies a time variation in global MRA relative to Marine13 with an amplitude of about 100 years in the Holocene. Thus, the ΔR values discussed in this work are not equivalent to ΔR values discussed in previous work (but, in the Holocene, Marine13 ΔR values can roughly be compared by adding 150 years to the Marine20 ΔR).

We begin by assessing the optimal ΔR through comparison of independent radiocarbon age models for each core, with uncertainty quantified using the Undatable age-depth modeling method (Lougheed and Obrochta, 2019), compared with independent ages for tephra events dated with terrestrial materials (**Supplementary Table S3**). There is uncertainty in the identification and appropriate ages for some tephra layers, with the most pronounced tephras in this interval, Saksunarvatn and Vedde, known to be originated from volcanic centers that experienced multiple geochemically similar eruptions over periods of ~500-1000 yrs (Harning et al., 2022; Jennings et al., 2014; Óladóttir et al., 2020). For example, three basaltic tephra layers in MD99-2322 between 9.9 and 10.4 ka are geochemically similar to the Saksunarvatn tephra (Jennings et al., 2014), which is consistent with the Saksunarvatn ash actually being part of a series of eruptions of the Grímsvötn volcanic system referred to as the G10ka series tephra (Óladóttir et al., 2020). Thus, these and other tephra horizons may be more appropriately used as time intervals rather than as precise markers. For our analysis, we first calculate age models for each core in radiocarbon years without calibration, quantifying uncertainty using Undatable (Lougheed and Obrochta, 2019). Then we compare the difference between cores predicted radiocarbon age ±1 sigma range for each tephra versus accepted terrestrial ages for each tephra, converted to an ±1 sigma radiocarbon age range from calendar years before present using the MARINE20 calibration curve (**Figure**

264 **2G**). Considering the Undatable quantified uncertainties of our age model and the uncertainties in the
265 tephra ages themselves, we find that a simple 0 yr MARINE20 ΔR provides good agreement (the
266 summed tephra-based estimate distributions have a central tendency of 1 yr). Previous PSV studies
267 found that a ΔR of ~130 yrs, but up to 250 yrs, is needed for the INTCAL04 Marine curve which has a
268 built in MRA correction of 400 yrs (Kristjánsdóttir et al., 2007) and a ΔR of 150 ± 50 yrs was needed for
269 the Marine13 curve (Nilsson et al., 2022) in order to fit the tephra age constraints. These ΔR choices are
270 consistent with our observations, given the different approach taken in construction of the Marine20
271 curve (**Supplementary Figure S3**).

272 While our uncertainties are large, there is some indication that ΔR may vary in this region as a function
273 of time. This is not surprising given that radiocarbon calibration curves are not designed for polar
274 regions where sea ice extent, ocean upwelling and air-sea gas exchange may cause larger changes
275 (Heaton et al., 2020; Reimer et al., 2013) and Holocene paleoceanographic reconstructions from the
276 North Iceland Shelf indicate water mass variability (Kristjánsdóttir et al., 2017). There is evidence from
277 shells for North Iceland shelf MRA variations on the order of about 100 years over the last 1,300 years
278 that are thought to be related to ocean circulation changes (Wanamaker et al., 2012). MRA variations
279 were likely largest prior to the onset of the Holocene, as suggested by the large >200 yr ΔR implied by
280 the ~12 ka Vedde Ash deposited in Core 2264 during the Younger Dryas (**Figure 2G**). Significant ΔR
281 variations in the North Atlantic during the deglaciation have been documented elsewhere. Using corals
282 in the Labrador Sea, Cao et al. (2007) found Younger Dryas aged waters had a ΔR ~200 yrs greater than
283 the Bølling–Allerød or Holocene. Bondevik et al. (2006) found a similar ~200 yr offset for the Younger
284 Dryas using paired terrestrial and marine materials from sediments deposited on the Norwegian Margin.
285 Additionally, Stern and Lisiecki (2013) demonstrated similar MRA changes using a network of North
286 Atlantic deep sea cores. With these observations in mind, for the purposes of this study we use a
287 constant ΔR of 0 ± 70 yrs for our final product. We feel that this is more straight forward than trying to
288 apply a variable ΔR and reduces the number of assumptions we need to make. However, we recognize
289 that on centennial timescales, time variations in ΔR are a large source of uncertainty in our age model
290 and that our ages are likely at least 200 yrs too old during the Younger Dryas. Future studies that use
291 this reconstruction as a tuning target may want to recalculate the age model based on their choice of ΔR
292 and its uncertainty and time variation (all data required to make these calculations are available in the
293 Zenodo database; doi: 10.5281/zenodo.7734229).

Finally, to reduce uncertainties associated with post-depositional remanent magnetization processes we only use sediment deposited at rates greater than 100 cm/kyr. We calculate the age models for each core using the MARINE20 curve and ΔR of 0 ± 70 yrs to calculate sedimentation rates (**Figure 2F**) and disregard intervals with accumulation rates less than 100 cm/kyr in further analyses (grey regions in **Figure 4**).

3.3 Stratigraphic Correlation

On each core's independent age model, sediments deposited at rates greater than 100 cm/kyr show excellent agreement on millennial timescales, but this correlation is less clear on shorter timescales (**Figure 4**). We assume some unknown proportion of the mismatches on these timescales is related to imperfect age models and resulting misalignment and some other proportion is related to noise introduced during remanence acquisition, coring, sampling, and/or measurement.

Previously, it has been demonstrated that alignment of PSV signals between Cores 2269 and 2322 on depth does not violate radiocarbon uncertainty and improves the correlation of percent carbonate data in each core (Hagen et al., 2020; Stoner et al., 2007). Using the reasonable assumption that both cores share a common geomagnetic history on these length scales (c.f., Korte et al., 2019), this alignment allowed reorganization of radiocarbon and tephra constraints from multiple sequences to a single regional correlated equivalent depth (CED) ultimately providing higher dating density to constrain the Greenland/Iceland PSV stack (Stoner et al., 2013). We apply the same principle here using objective alignments determined using the PSV Dynamic Time Warping (DTW) algorithm of Hagen et al. (2020). This DTW algorithm, modified from that of Hay et al. (2019), utilizes dynamic programing to generate a library of potential alignments that minimize the cumulative angular difference (quantified as the cosine distance) between vector time series while varying two parameters that control how variable sediment accumulation rates can be (g value) and how much the two records overlap (edge value). Considering cosine distance of the vectors instead of simply using inclination and/or declination is particularly useful for studies of higher latitude PSV like this, as, when the field is steeply dipping and inclination is near 90°, small angular changes in the vector can result in large declination changes. The resulting library of possible DTW solutions can then be evaluated in geologic context and with statistical tests to find the optimal solution(s) (Hagen et al., 2020). Other DTW algorithms have previously been used to prepare data for single variable stacks, like benthic $\delta^{18}O$ (Lisiecki and Raymo, 2005) and relative paleointensity

(Channell et al., 2009). However, this is the first time this approach has been applied to building a radiocarbon dated PSV vector stack.

First, we develop a target curve and CED scale for the DTW alignment using Cores 2269 and 2264. Core 2269 is used for the last ~11 kyr as it has the most linear apparent accumulation rates (<20.86 m depth in the core) and Core 2264 is used below that as it goes the furthest back in time (>5 m depth in the core, offset by 15.865 m), with the overlap determined using a prominent PSV feature (**Figures 2 and 5**). Next, Cores 2322, 2265, and 2266 were aligned to this target curve using the PSV DTW algorithm. The library of potential alignments between Cores 2322 and 2269 were previously presented by Hagen et al. (2020) and the best fit was determined by considering the highest cross correlation with sufficient overlap within the parameter range that showed statistical significance when comparing algorithm results for the data versus alignment to synthetic randomly generated PSV curves. We perform identical analyses using Cores 2265 and 2266 and similarly assess the DTW results, choosing the best fits that meet the same criteria as used by Hagen et al. (2020) (**Figure 5A-C; Supplementary Figure S4**). Transferring each core's radiocarbon dates from their original depth to the regional CED scale provides confidence in this approach, with radiocarbon dates falling in stratigraphic order (**Figure 5D**). This high density of 71 dates from the intervals of the cores with >100cm/kyr accumulation rates, averaging one date every 210 yrs although unevenly distributed in time, provides a higher resolution age model than would be possible with any core alone (**Figure 5E**).

3.4 The GREENICE15k Stack

Paleomagnetic data were stacked on the DTW aligned CED scale using the Gaussian weighted moving window method described by Reilly et al. (2018) at 10 year time increments using a Gaussian function with 30 yrs full width at half maximum. Due to the magnetometer response function, successive u-channel data are not independent. Accordingly, the N value used in the calculation of the Fisher statistics is the number of cores that contribute to each time increment, not the number of measurements, so that uncertainty estimates are not artificially suppressed (Reilly et al., 2018). Declinations for each core were rotated to a mean of zero, assuming that each core spans enough time that they average to a geocentric axial dipole. This assumption is likely imperfect and absolute declination remains an unconstrained uncertainty in the final stack; however, we choose this approach as it provides a reasonable agreement between cores (**Figure 5A**) and requires the least number of assumptions. Ages were determined for each core on their CED scale using the combined radiocarbon

dataset using the Undatable algorithm, an *x-factor* = 0.1, the Marine20 calibration curve, and ΔR = 0 ± 70 yrs (Heaton et al., 2020; Lougheed and Obrochta, 2019) (**Figure 5E**). The result is a 15 kyr inclination and declination reconstruction with centennial resolution. α95 values are lowest between ~3 and 11 ka, where the stack is constrained by the greatest number of overlapping cores, as α95 is a function of $1/\sqrt{N}$ (**Figure 5I**). Uncertainties that we are unable to constrain include the absolute declination rotation and where the stack is only constrained by a single record in the last ~1 kyr (2269) and in the time older than ~12 ka (2264). For the time periods constrained by only one core, α95 values are calculated from only the single core values within the ~30 yr wide interval. These α95 values are typically higher as N = 1, but could also have unquantified errors inherent to sediment paleomagnetic records (see Section 1) that could be addressed in future work with replication from other sedimentary archives. On centennial timescales, unaccounted for variations in ΔR beyond the ± 70 yrs used in the age model are another source of uncertainty, particularly ~11-13 ka during the Younger Dryas where reservoir effects are likely 200 yrs or more than the constant ΔR used here.

4. Discussion

4.1 Fidelity of the GREENICE15k Reconstruction

Thompson (1984) and Peck et al. (1996) outline a number of reliability criteria used to assess if directional changes in sediment PSV accurately reflect the geomagnetic field, related to the quality of the magnetizations and, perhaps more importantly, the reproducibility of the signal on a variety of levels, as discussed below.

The magnetizations of the cores presented here have well-defined ChRMs with low MAD (<5°) values that demagnetize towards the origin carried by (titano)magnetite (**Figures 2 and 3**; Andrews et al., 2003; 2008; Hatfield et al., 2019; Stoner et al., 2007). Hysteresis data in MD99-2269 and MD99-2322 are consistent with well characterized nearby core top samples (Hatfield et al., 2019), stream sediments from nearby Iceland and Greenland margin source regions (Hatfield et al., 2013; 2017), and regional North Atlantic sediments that have previously yielded quality paleomagnetic records (Kissel et al., 1999; 2009; Snowball and Moros, 2003; Ballini et al., 2006; Evans et al., 2007) (**Figure 3C**). Previous work demonstrated that there is a strong inverse correlation between magnetic susceptibility and weight

384 percent $CaCO_3$ in Cores JM96-1232 (collected near MD99-2264), MD99-2269, and MD99-2322 with low
385 $CaCO_3$ and high magnetic susceptibility common in late deglacial and early Holocene sediments when
386 terrigenous flux was highest to both the Greenland and Iceland margins (Andrews et al., 2003; 2008;
387 Stoner et al., 2007). Down core NRM intensity variations (**Figure 2A**) are largely controlled by the
388 concentration of ferrimagnetic minerals driven by changes in lithogenic versus biogenic composition.

389 The >100 cm/kyr accumulation rates required for the construction of this stack should be high enough to
390 resolve centennial to millennial trends in PSV with minimized complications from post-depositional
391 remanent magnetization (pDRM) acquisition processes and smoothing by the response function of the
392 magnetometer while make u-channel measurements. The accumulation rates required to resolve
393 centennial variations in PSV are likely higher than typically needed for paleoclimate reconstructions
394 (Anderson, 2001), as magnetizations are thought to be acquired over a lock-in zone that acts as a low
395 pass filter (e.g., Balbas et al., 2018; Lund and Keigwin, 1994; Roberts and Winklhofer, 2004) and can
396 cause offsets in the paleomagnetic signal of 0-25 cm in marine sediments (Channell and Guyodo, 2004;
397 Hagen et al., 2020; Simon et al., 2018; Stoner et al., 2013; Suganuma et al., 2010; Tauxe et al., 1996).
398 While the exact lock-in offset is unknown and unable to be tested here, its impacts are likely minimal for
399 the purposes of this study and we can approximate its effect using a reasonable estimate of 15 cm. With
400 this offset, the maximum offset in time for our stack would be 150 yrs for sediments deposited at 100
401 cm/kyr and on sub-centennial timescales for the majority of the sediments deposited >100 cm/kyr that
402 contribute to our stack (see **Figure 2F**).These are essentially the same timescales of uncertainties
403 associated with our radiocarbon age model and choice of ΔR.

404 The greatest uncertainties more likely stem from coring/sampling disturbance or noise inherent to the
405 magnetic acquisition process related to variations in sedimentation and/or bioturbation. So perhaps the
406 best reliability criteria for this region is to assess PSV reproducibility to provide the strongest support for
407 the fidelity of a PSV signal on a variety of scales, from the sample level, to basin level, to regional level.
408 On a sample and basin level, being that these and likely other high-accumulation rate depocenters on
409 the North Iceland and Southeast Greenland shelves have proven to be high fidelity PSV archives, it
410 would be worthwhile for future coring efforts to re-core these basins with multiple cores to better
411 quantify the uncertainty of the PSV signals at each core location and to better capture the latest
412 Holocene sediments. On a regional level, where these cores overlap, we find that signal must be well
413 reproduced, as the objective alignments accomplished with the DTW algorithm agree especially well
414 with the radiocarbon constraints (**Figure 5**).

One major contribution of the GREENICE15k stack is the extension to 15 ka through MD99-2264, which provides a longer perspective on geomagnetic change and can serve as a PSV template through the abrupt Bølling–Allerød and Younger Dryas climate transitions. As mentioned earlier, uncertainties within the 12-15 ka interval are also difficult to constrain as only one core is used in this interval. It is, of course, increasingly difficult to recover ultra-high resolution sediments the further one moves back in time using surface coring devices. However, Core JM96-1215/2GC, taken near MD99-2322 in the Kangerlussuaq Trough, is an incomplete record, but captures an interval of expanded deglacial accumulation rates (Jennings et al., 2006, 2002) and seemingly well-resolved inclination and declination (Jennings et al., 2014). While the 6 m JM96-1215/2GC does not meet our accumulation rate and radiocarbon criteria for inclusion in this study, correlation of the JM96-1215/2GC directional record to the GREENICE15k stack using the objective DTW algorithm of Hagen et al. (2020) illustrates that it captures the major ~11.5-14 ka GREENICE15k PSV features with variation consistent with available ^{14}C dates, considering previously recognized complications (Jennings et al., 2006) (**Figure 6**). This includes a ~500 yr interval around 13 ka where the field was steeply dipping over the Northern North Atlantic, characterized by >85^{o} inclinations and large variation in declination. The large variations in declination, highlighted in pink shading in **Figures 6A, 7C, and 8**, are likely in part a reflection of the uncertainties in the paleomagnetic data themselves. For example, at inclinations of 85^{o} with an α95 of 10^{o}, as estimated around 13 ka in GREENICE15k (**Figure 5I**), the 95% confidence interval for declination would be 155^{o}.

There are few high-resolution (>50 cm/kyr) PSV records in the circum-Northern North Atlantic region that extend back to 15 ka to compare to (**Figure 7**). Some of the sites that do exist include Eastern USA Lake records, including Lake Seneca and Sandy, that span the last ~13.5 kyr (King and Peck, 2002), a combination of Northern European sediments from Finland, Sweden, Russia, and the Baltic Sea that include stacks that span 0-10 ka and 11-14 ka (Haltia-Hovi et al., 2010; Lougheed et al., 2014), and the Meerfelder Maar PSV record from Germany that spans the entire studied interval (Stockhausen, 1998). The SHADIF14k spherical harmonic model extends back to 14 ka using only archeomagnetic and lava flow data, although 83% of the data that constrain this model span only the last 3 kyr and only 3% of the data used span the 8 - 14 ka interval (Pavón-Carrasco et al., 2014). The GGF100k model spans this interval, however it is also limited by available data and has low temporal resolution as the model is focused on modeling longer-period variations (Panovska et al., 2018). For the purposes of these comparisons, all records are relocated via their VGP paths to Reykjavik, Iceland in **Figure 7** to account for geometric effects on the inclination and declination signals (c.f., Korte et al., 2019). This transformation would be valid if Earth's magnetic field was a pure dipole that deviates (or wobbles) from the axis of

447 rotation (i.e., it could be described with just the spherical harmonic degree 1 coefficients). Of course,
448 the field is more complicated than this and on these length scales, differences could be explained by
449 non-dipole contributions in addition to chronological and paleomagnetic uncertainties. While
450 GREENICE15k has superb resolution in both the paleomagnetic signal and chronology (**Figure 5**), some of
451 the other records may be further complicated by pDRM smoothing due to their lower accumulation
452 rates and more limited chronological constraints.

453 We find some broad similarities in our regional comparison, acknowledging issues in chronology and
454 record resolution. As previously noted by Ólafsdóttir et al. (2019) there is good agreement between
455 North Iceland PSV records and the Finnish Lake stack of Haltia-Hovi et al. (2010) in the Holocene if the
456 records are relocated to common geographic coordinates (**Figure 8**). This comparison also seems to
457 hold for the deglacial Fennoscandia PSV stack of Lougheed et al. (2014), including evidence for a steeply
458 dipping field over the Northern North Atlantic ~13 ka. In general, while the timing of features generally
459 agrees with centennial uncertainty, the amplitude of declination changes is significantly less and
460 inclination values are somewhat shallower for the Holocene Finnish Lake stack. Some of the differences
461 are likely related to non-dipole contributions to the field, but others may be related to other difficult to
462 assess uncertainties related to coring artifacts, chronology, smoothing as a result of post-depositional
463 remanence acquisition in these lower accumulation rate sediments (~50-75 cm/kyr) and/or depositional
464 and magnetic recording complexities. Even with our density of radiocarbon dates, there are still likely
465 chronological uncertainties on the order of ~100-200 years related to uncertainties in the radiocarbon
466 method itself and unknown time variations in ΔR, particularly during the deglacial time.

467

468 ## 4.2 Amplitude and Timescale of PSV

469 To investigate the amplitudes and timescales of PSV in the Northern North Atlantic, we first convert
470 inclination and declination into a single parameter, angular deviation from what would be expected if
471 the Earth was a geocentric axial dipole (GAD). This was done for the GREENICE15k stack, the 5 records
472 used in constructing the stack, a suite of site predictions from published time varying spherical harmonic
473 models (Constable et al., 2016; Jackson et al., 2000; Nilsson et al., 2022; Panovska et al., 2018; Pavón-
474 Carrasco et al., 2014), and a nearby deep sea sediment record with a long and continuous PSV
475 reconstruction, ODP Site 983 (Channell, 1999; Channell et al., 1997) (**Figure 9**). Time series analysis was
476 performed using the multi-taper method using the MATLAB implementation of Husson et al. (2014).

The GREENICE15k stack agrees well with the variance of the five individual records at millennial and centennial timescales but has significantly less variance at decadal timescales (**Figure 9A**). This is not surprising as this high frequency variance could be noise in the individual records that is removed by the 30 yr wide filter used in our stacking process (see Section 3.4) or high frequency geomagnetic field behavior that is not resolved with our stacking and chronologic methods. As it is likely some combination of both, new dedicated efforts to recovered parallel cores at each location would be required to assess reproducibility at this level. At millennial and centennial timescales, the variance in the cores are generally in agreement with the stack with some minor differences. Core 2264 consistently has the greatest variance but is biased towards the high amplitude PSV observed in the 11-15 ka interval (**Figures 4, 6, 8 and 9A**). Cores 2265 and 2266 generally have lower variance but are shorter in duration and biased towards the lower amplitude PSV observed in the 3.5 -11 ka interval (**Figures 4, 8 and 9A**). This indicates that individual records that only span a few thousand years may not be representative of long term variance. Given these comparisons, we argue that the GREENICE15k stack does a good job of capturing the variance of PSV in the Northern North Atlantic at centennial and millennial timescales, with highest confidence in the <12 ka interval where the stack is constrained by multiple cores.

The variance of the GREENICE15k stack at decadal timescales is difficult to assess given the limits of our methods. However, comparisons with GUFM1 model predictions (Jackson et al., 2000) constrained by 400 years of historical observations, have been previously used to be representative of variance on this timescale for intensity changes (e.g., Sadhasivan and Constable, 2022) and could be instructive. The GREENICE15k stack has similar but higher variance than GUFM1 at decadal timescales if the entire 0-15 ka portion is used, but is nearly identical if only the 0-12 ka portion that is constrained by multiple cores is used (**Figure 9B**). The difference could be noise at this timescale in the MD99-2264 record even after it is smoothed by the 30 yr filter in our stacking procedure (**Figure 9A**). However, It is also difficult to assess how representative the decadal scale variance in the 400 yr GUFM1 reconstruction is when compared to longer geomagnetic change. Thus, as discussed in the comparison with individual cores, even though the decadal variance of GREENICE15k is consistent with variance in the GUFM1 reconstruction, it is difficult to separate decadal scale signal and noise in PSV even with these very well dated and high-resolution sediment cores.

Variance at centennial timescales in our stack is consistently higher than Holocene time varying spherical harmonic models, although many of the models come close or agree to the variance of our

stack at millennial timescales (**Figure 9B**), particularly the pfm9k.2 model of Nilsson et al. (2022). These comparisons reinforce the fact that the current state of the art geologically constrained geomagnetic field models do a good job at capturing longer period variation of the field, but are missing the centennial scale variations that can be captured in very high resolution sediment records. Continued work to develop globally distributed sedimentary records with strong chronologies, optimally >100 cm/kyr sedimentation rates, and regional reproduction is needed to improve modeling efforts of the sub-millennial dynamics of the geomagnetic field. Sub-millennial timescales are important to consider, as they are likely the same timescales over which dynamic geomagnetic features such as south Atlantic anomaly type events (Nilsson et al., 2022), regional geomagnetic intensity changes (e.g., geomagnetic spikes; Shaar et al., 2022), geomagnetic excursions (Nowaczyk et al., 2012) and perhaps even reversals operate on. We hypothesize that some of these 0-15 ka Northern North Atlantic sub-millennial PSV variations are likely a reflection of rapid sub-millennial regional intensity variations, like those documented in the Levant region (Shaar et al., 2022) (**Figure 10**). Where the Levant Archeomagnetic Intensity Curve (LAC) and GREENICE15k overlap, we observe easterly GREENICE15k VGPs over Eurasia around 50^{o} east during periods of LAC paleointensity highs and more westerly GREENICE15k VGP longitudes during LAC paleointensity lows. GREENICE15k VGP latitudes reach exceptionally low values between 2500 and 3000 cal yrs BP, approaching 50^{o} N over Eurasia near the end of this period, during the very high paleointensity intervals of the LAC 'geomagnetic spike' (**Figure 10**). The amplitude of the ~2500 BP GREENICE15k VGP latitude minimum is likely robust, as it is driven by the large declination feature reproduced in MD99-2266, MD99-2269, and MD99-2322 (**Figure 4**). Given these observation, we might also predict that there were similar intensity variations during past times of eastern VGP longitudes and low VGP latitudes, like we observe around 11,500 and 13,000 cal yrs BP.

There are likely lower frequency variations of geomagnetic change that cannot be captured by a 15 kyr record. While our record has significantly higher variance at all timescales than the GGF100k model that is designed to study longer period variations of the field (Panovska et al., 2018), the nearby deep sea sediment record ODP Site 983, recovered from the Gardar Drift south of Iceland and deposited at ~14 cm/kyr mean sedimentation rates has similar variance at millennial timescales (**Figure 9C**). The similarity at this timescale may suggest moderate resolution deep sea PSV records like these may be suitable for PSV stratigraphy at millennial resolution, however it may also indicate that 15,000 years is not long enough to fully resolve millennial scale geomagnetic variance and that the generally high intensities of last 15,000 may not be truly representative of the long-term geomagnetic field (e.g., Wang et al., 2015). The ODP Site 983 record shows significantly higher variance at multi-millennial timescales

than GREENICE15k, suggesting there are likely lower frequency but high amplitude variations or unidentified variations in mode behavior that are not captured in our relatively short stack.

5. Conclusion

GREENICE15k is a very high resolution and well-dated inclination and declination PSV stack that captures 15 kyr of centennial and millennial scale geomagnetic variability in the Northern North Atlantic. These results validate and improve upon prior results, while providing additional geochronological constraints with modern radiocarbon calibration and reservoir age considerations and demonstrating the reproducibility of the PSV signal including its amplitude. Furthermore, GREENICE15k provides a well dated template of geomagnetic change that extends through abrupt climate variability of the last deglaciation and can be used to assess or constrain regional deglacial to Holocene chronologies in future studies. In general, our results are similar to predictions from global reconstructions, but have higher amplitude of variability, particularly at sub-millennial timescales. While millennial scale variability of the geomagnetic field is often captured in field models and globally distributed sedimentary records, sub-millennial scale variability, like that captured in the GREENICE15k stack, has been much more difficult to reconstruct. This is because the full amplitude of centennial scale variation is often attenuated in lower resolution sediment records or, in the case of very high resolution records, it has been challenging to demonstrate reproducibility of centennial scale variability on a regional scale.

Although the amount of variance at centennial and decadal scales over longer geologic time remains uncertain, the GREENICE15k stack is consistent with decadal and centennial variance observed in the 400 year historical reconstruction of the GUFM1 model (Jackson et al., 2000). Furthermore, similar to the LAC high-resolution paleomagnetic intensity reconstruction of Shaar et al. (2022), our findings highlight the potential for dramatic regional scale geomagnetic variability on sub-millennial timescales. A more comprehensive understanding of these sub-millennial timescales using sedimentary records like we present here is important for advancing our knowledge of some of the most intriguing features of the geodynamo, like south Atlantic anomaly-like features, geomagnetic spikes, excursions, and reversals.

Acknowledgements

Brendan Reilly and Joseph Stoner were supported by National Science Foundation awards EAR-1645411 and OCE-2300114. Data are available in Magic (doi: 10.7288/V4/MAGIC/19300 and 10.7288/V4/MAGIC/19360) and Zenodo (doi: 10.5281/zenodo.7734229). PSV Dynamic Time Warping code is available through GitHub (https://github.com/CedricHagen/PSV-dynamic-time-warping). We thank Bernie Housen and Cristina Garcia-Lasanta for their help collecting hysteresis data at Western Washington University. We thank editor Mark Dekkers, associate editor Daniel Pastor-Galán, reviewer Ron Shaar and an anonymous reviewer for their insightful and constructive suggestions.

Figures

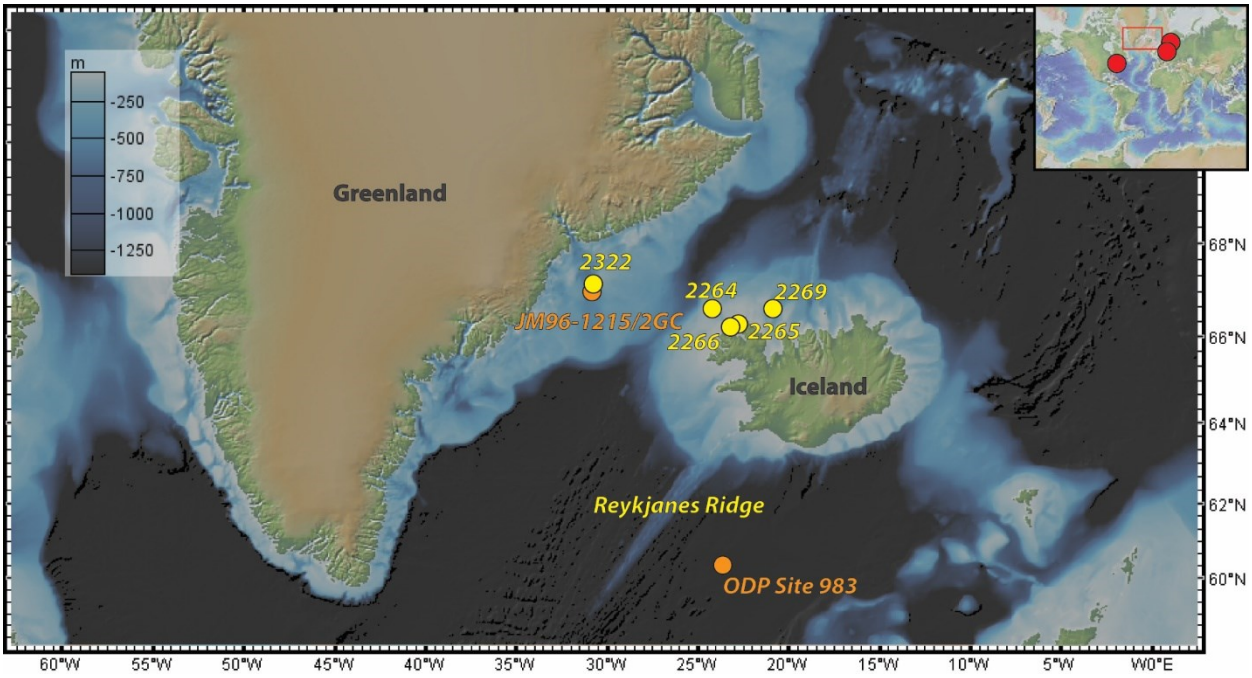

Figure 1. Map. Sediment core locations from the Northern North Atlantic (NNA), including those studied here (yellow), additional NNA sites discussed in the text (orange), and more distal PSV records that extent back to 15 ka at moderate to high resolution (red). This map was created using the Global Multi-Resolution Topography (GMRT) synthesis and GeoMapApp (Ryan et al., 2009).

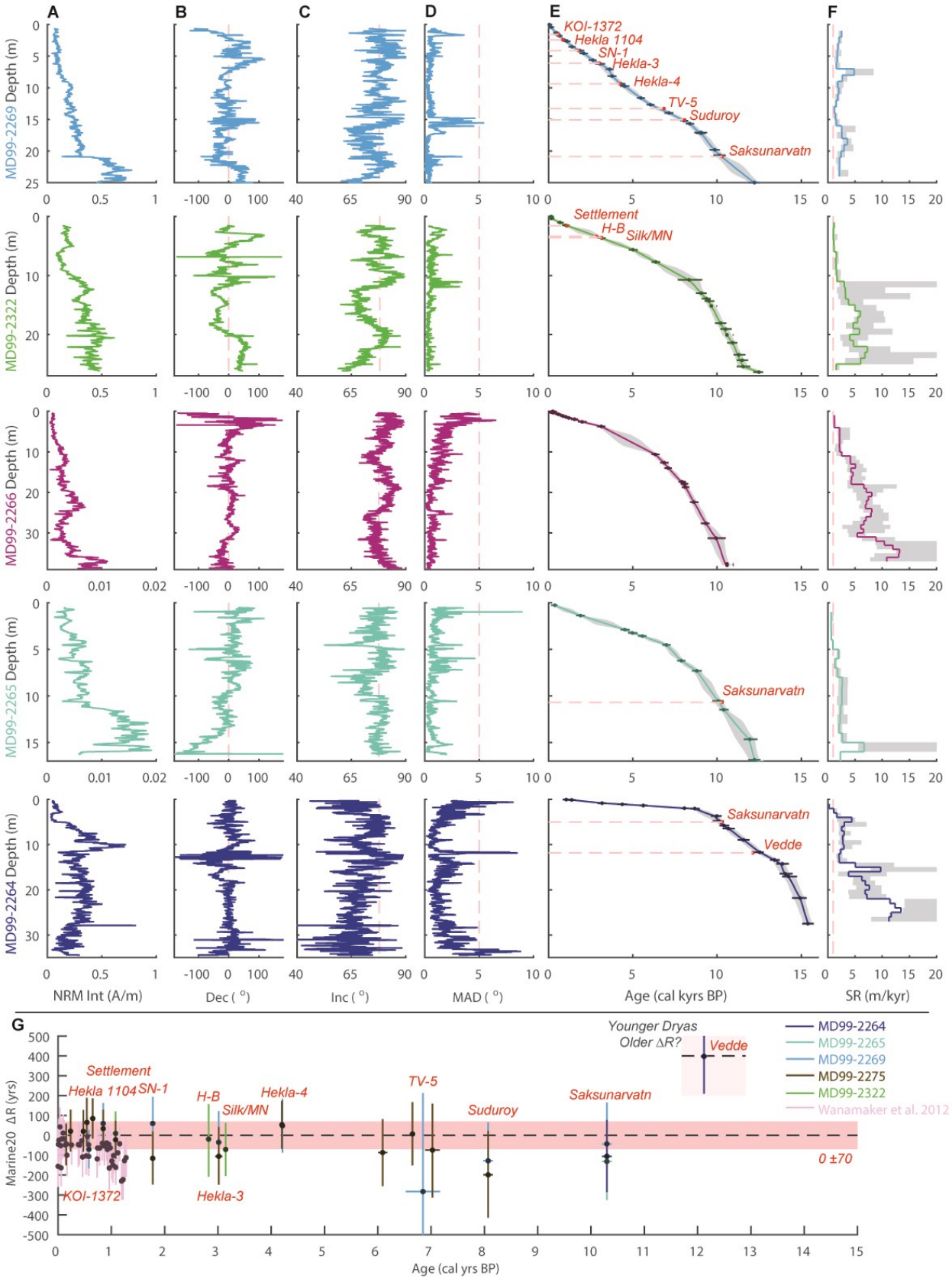
A
B
C
D
E
F
MD99-2269 Depth (m)
MD99-2322 Depth (m)
MD99-2266 Depth (m)
MD99-2265 Depth (m)
MD99-2264 Depth (m)
KOI-1372
Hekla 1104
SN-1
Hekla-3
Hekla-4
TV-5
Suduroy
Saksunarvatn
Settlement
H-B
Silk/MN
Vedde
NRM Int (A/m)
Dec (°)
Inc (°)
MAD (°)
Age (cal kyrs BP)
SR (m/kyr)
G
Younger Dryas
Older ΔR?
MD99-2264
MD99-2265
MD99-2269
MD99-2275
MD99-2322
Wanamaker et al. 2012
Marine20 ΔR (yrs)
0 ±70
Age (cal yrs BP)

584

Figure 2. Paleomagnetic data on depth, age models, and constraints on radiocarbon reservoir age. (A) Natural Remanent Magnetization (NRM) intensity. **(B)** Characteristic Remanent Magnetization (ChRM) declination rotated to a mean of zero. Vertical dash line = 0^{o}. **(C)** ChRM inclination. Vertical dashed line is the predicted value based on the geocentric axial dipole (GAD) hypothesis. **(D)** ChRM MAD value. Vertical dashed line at 5^{o}, for which values below are considered to be very well defined magnetizations. **(E)** Marine20 calibrated radiocarbon based age models (ΔR = 0 ± 70 yrs). Colored solid line is median age model. Gray shading is the ±2σ interval. Black dots/horizontal lines are the calibrated radiocarbon constraints and ±2σ interval. Horizontal red dashed lines indicate tephra horizons for which there are terrestrial radiocarbon or ice core ages and red dots indicate the mean independently derived ages. **(F)** Sedimentation rate (SR). Colored line is median estimate. Gray shading is ±1σ interval. Vertical dashed line indicates 1 m/kyr. **(G)** Estimates of Marine20 ΔR from tephra layers found in five sediment cores from the north Iceland and southeast Greenland continental shelves (four cores discussed in this study, plus the tephra record of MD99-2275; Eiríksson et al., 2004; Gudmundsdóttir et al., 2011) and north Iceland shelfs clam shells (29 shell records). Shells were absolutely dated using cross dating techniques derived from dendrochronology (Wanamaker et al., 2012). Dark horizontal red shading indicates the ΔR used in this study. Lighter horizontal red shading indicates a possible older ΔR during the Younger Dryas interval.

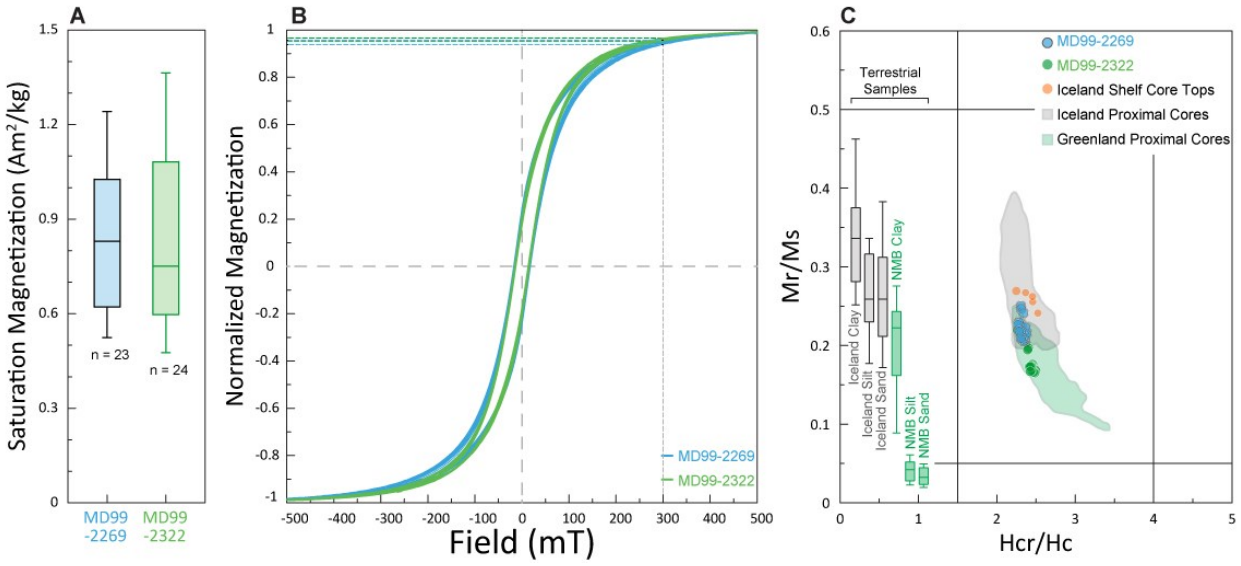

Figure 3: Hysteresis data for the Southeast Greenland (MD99-2322) and North Iceland Shelves (MD99-2269). (A) Box whisker plot of mass normalized saturation magnetization (M_s) values showing the median (center line), upper and lower quartiles (box), and full range of values (whiskers). **(B)** Normalized magnetic hysteresis loops following paramagnetic correction, colored dashed lines show the range of normalized magnetization values acquired in a 300 mT field. **(C)** Day plot of measured core samples (green and blue symbols). These values cluster tightly and fall within the range of previous cores taken from the Greenland and Iceland margins (shaded areas) as summarized by Hatfield et al. (2013; 2019) and include original data from Iceland proximal cores SU90-33 and PS2644-5 (Kissel etal.,1999), SO80-05, SO82-07 and LO09-18 (Snowball and Moros,2003), MD99-2247 (Ballini et al.,2006), MD03-2674, MD03-2678, MD03-2684, MD03-2680, and MD03-2676 (Kissel et al., 2009), and Iceland Basin core tops (Hatfield et al., 2019) and Greenland proximal cores SU90-24 and SU90-16 (Kissel etal.,1999), MD99-2244 (Ballini et al.,2006), and MD99-2227 (Evans et al.,2007). The core samples also fall within the terrestrial sediment sources (box whiskers) from Iceland (gray) and from the proximal Nagssugtoqidian Mobile Belt (NMB; green), Greenland (Hatfield et al., 2017).

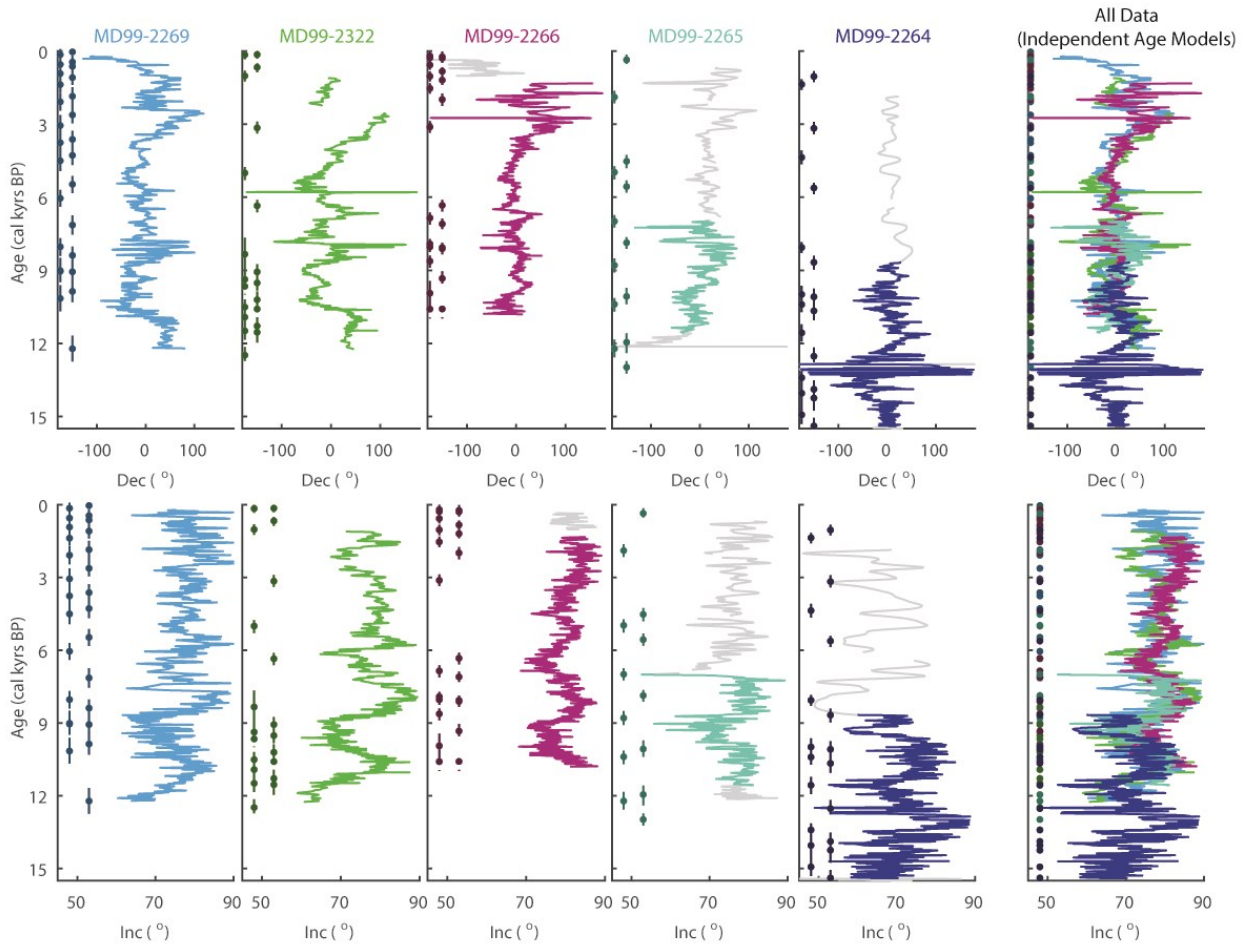

618

619 **Figure 4. Paleomagnetic data on independent radiocarbon age models.** ChRM declination (top row)
620 and inclination (bottom row) with locations of radiocarbon constraints indicated, offset in two columns
621 to improve visibility. Paleomagnetic data with colored lines are intervals with sedimentation rates
622 greater than 1 m/kyr used in this study, while gray intervals have lower sedimentation rates and were
623 not used in this study.

624

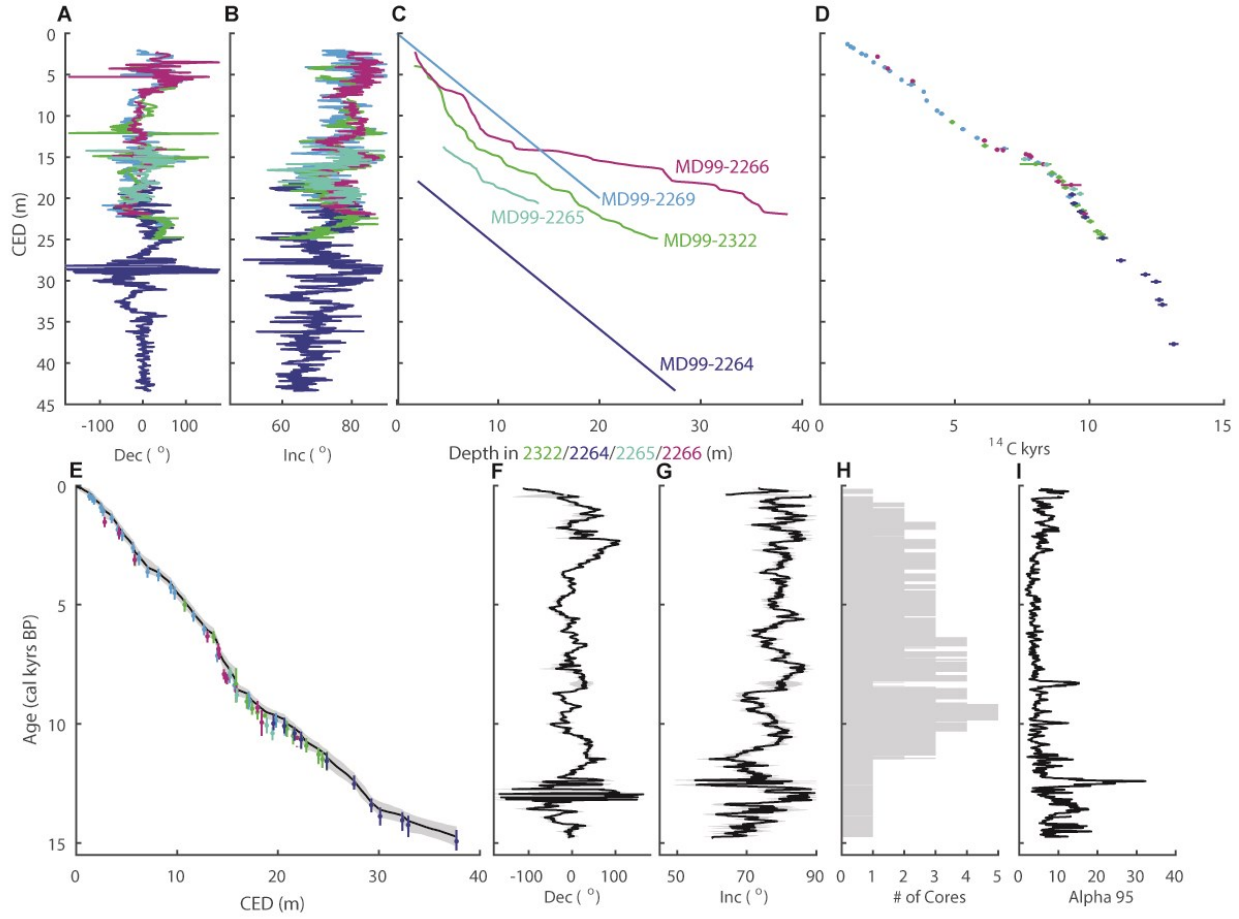

Figure 5. Stratigraphic correlation, regional age model, and paleomagnetic secular variation stack. (**A, B**) ChRM declination and inclination on correlated equivalent depth (CED) scales. (**C**) CED depths relative to original coring depths, with MD99-2322, 2265, and 2266 derived via Dynamic Time Warping (Hagen et al., 2020) and MD99-2264 via simple offset. DTW results for Core MD99-2322 were previously discussed by Hagen et al. (2020). DTW results for Cores MD99-2264 and 2265 are presented in **Supplemental Figure S4**. The depth scale of MD99-2269 was not changed. (**D**) Radiocarbon constraints transferred to the CED scale. (**E**) Marine20 calibrated age model for the combined radiocarbon data. (**F, G**) Stacked declination and inclination with the Fisher mean (black line) and ±1σ uncertainty (gray shading). (**H**) Number of cores that contributed to each horizon of the stack. (**I**) α95 of the Fisher mean.

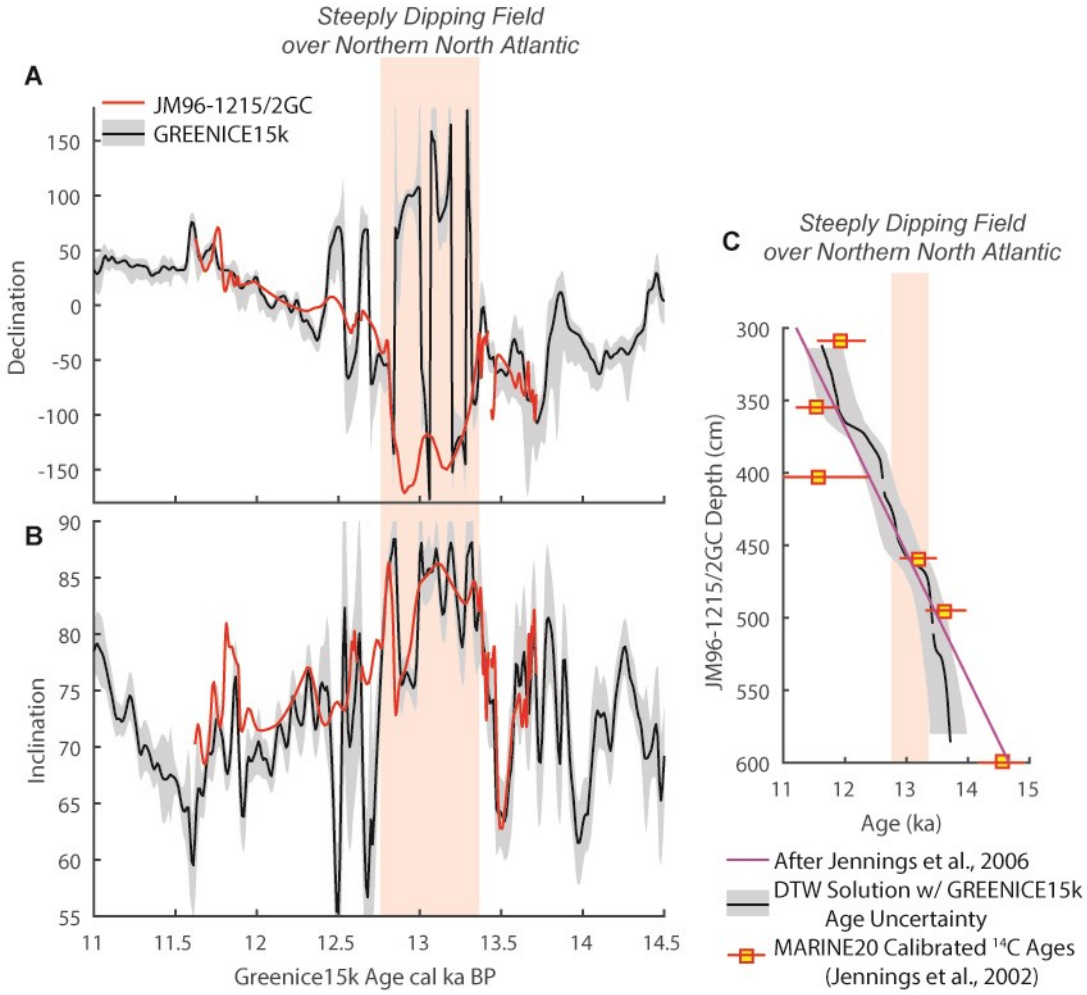

Figure 6. Comparison to JM96-1215/2GC, Kangerlussuaq Trough. (A) Declination and **(B**) inclination for the GREENICE15k stack (black) with ±1σ uncertainty (gray) compared with the directional record of JM96-1215/2GC (red; Jennings et al., 2014) transferred to PSV age through Dynamic Time Warping (DTW) using the method of Hagen et al. (2020) in the latest Pleistocene. **(C)** Age-depth plot comparing JM96-1215/2GC MARINE20 calibrated radiocarbon constraints (Jennings et al., 2002), with the linear age model used by Jennings et al. (2006; updated using MARINE20 and identical ΔR of this study), and the DTW correlation to GREENICE15k age with age uncertainty (**Figure 5E**) propagated. Light red shading indicates time interval of a steeply dipping geomagnetic field over the Northern North Atlantic ~13 ka. The declination mismatch in **A** around 13 ka is likely the result of this steeply dipping field, where small angular differences in the paleomagnetic vector can result in large declination differences.

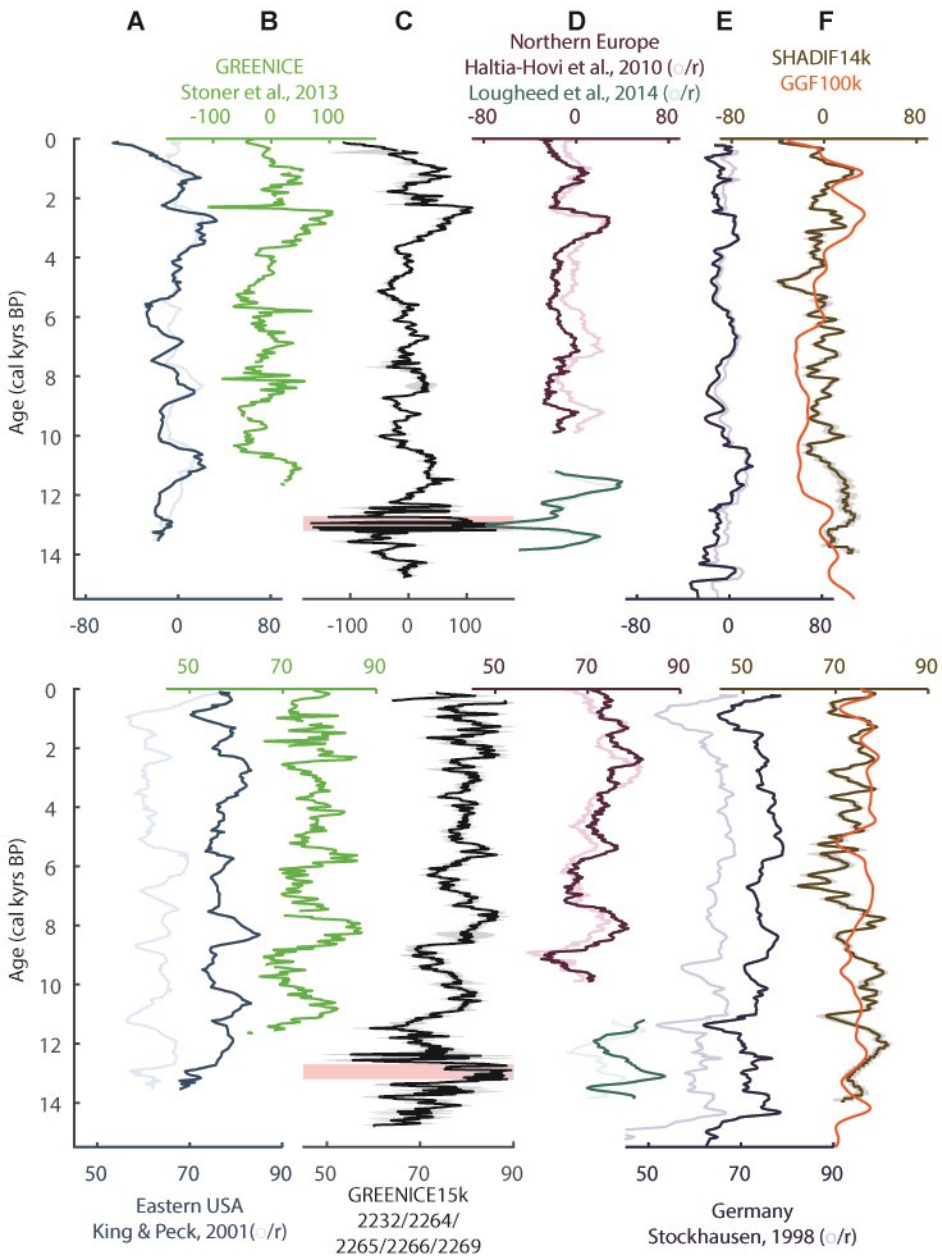

Figure 7. Comparison to regional records. (A) Eastern USA PSV stack, using data from LaBoeuf Lake, Seneca Lake, and Sandy Lake (King and Peck, 2002). **(B)** The original GREENICE Stack, using data from MD99-2269 and 2322 only (Stoner et al., 2013, 2007). **(C)** The new Northern North Atlantic PSV Stack, GREENICE15k, with red shading indicating interval with inclinations near 90^{o}. **(D)** Finnish Lake PSV stack, using data from Lake Lehmilampi and Lake Kortejärviä (Haltia-Hovi et al., 2010). Deglacial PSV stack for Fennoscandia, using data from Halsjön, Northwest Russia outcrops, and Lake Onega (Lougheed et al., 2014). **(E)** PSV from Meerfelder Maar, Germany (Stockhausen, 1998). **(F)** Model predictions for Reykjavik, Iceland from the archeomagnetic constrained SHA.DIF.14k (Pavón-Carrasco et al., 2014) and

GGF100k (Panovska et al., 2018). For the Eastern USA and European PSV data, lighter colors are the original data/stacks (o) and darker colors are those data relocated to Reykjavik, Iceland via their VGP paths (r).

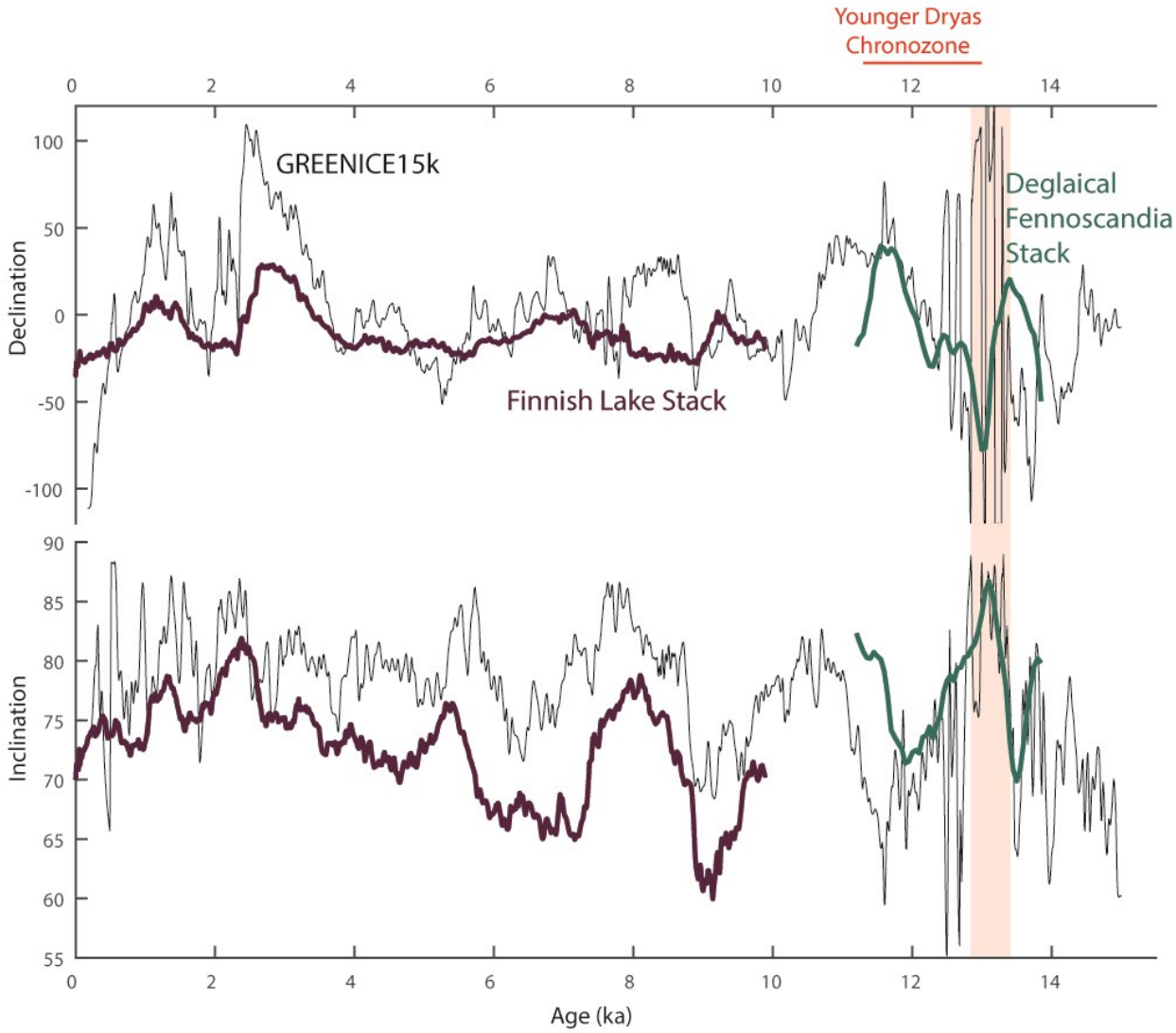

661

662 **Figure 8. Comparison of GREENICE15k to Northern European Records.** The Finnish Lake stack (purple),
663 using data from Lake Lehmilampi and Lake Korteäjrvi, is dated by counting annual layers back to 5.1 ka,
664 while the older sediments were dated by correlation to the varve-dated Lake Nautajärvi (Haltia-Hovi et
665 al., 2010). The deglacial PSV stack for Fennoscandia (teal), using data from Halsjön, Northwest Russia
666 outcrops, and Lake Onega, is dated through a variety of methods (Lougheed et al., 2014). Both records
667 are relocated to Reykjavik, Iceland via their VGP paths. Differences between the two records could be
668 related to non-dipole contributions to the field, uncertainties in chronology, geologic or sampling noise,
669 and magnetic acquisition processes. The Younger Dryas Chronozone is indicated as a time around which
670 there are known uncertainties in ΔR in the Northern North Atlantic.

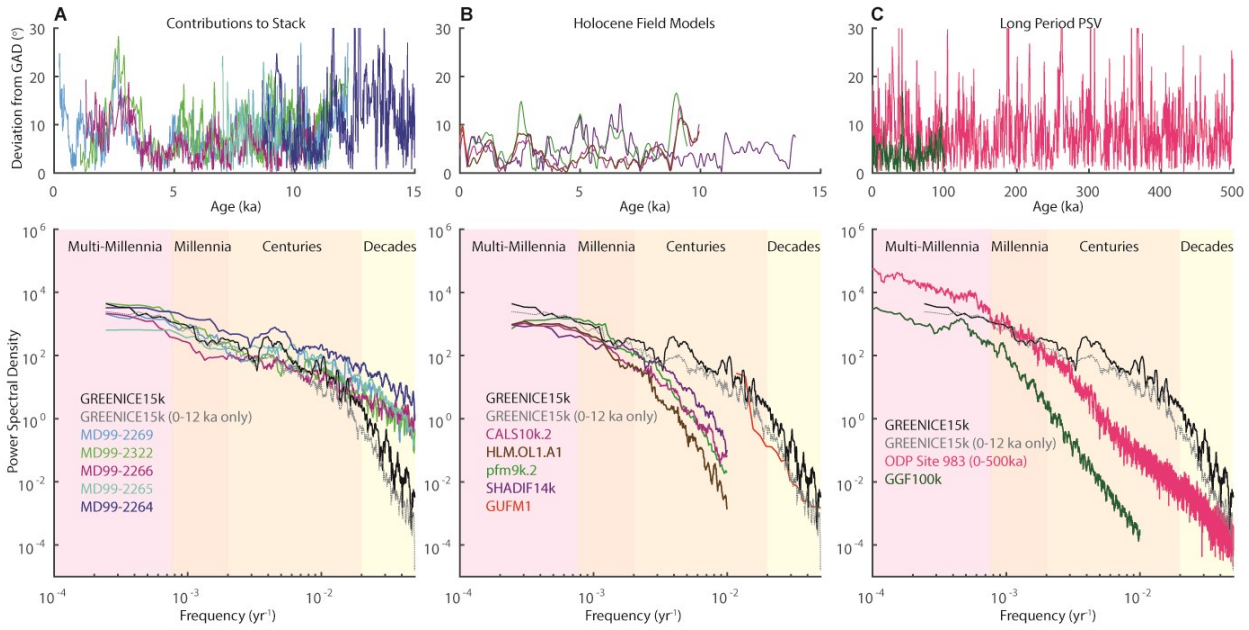

671

672 **Figure 9. Timescales of PSV variance in the Northern North Atlantic.** Angular deviation from the
673 predicted values of a geocentric axial dipole (GAD) as a function of time (top row) and frequency
674 (bottom row). **(A)** Comparison of the individual records discussed in this study and the GREENICE15k
675 stack. **(B)** Comparison with the CALS10k.2, HFM.OL1.A1 (Constable et al., 2016), pfm9k.2 (Nilsson et al.,
676 2022), SHADIF14k (Pavón-Carrasco et al., 2014), and GUFM1 (Jackson et al., 2000) Holocene field model
677 predictions for Reykjavik, Iceland. **(C)** Comparison with the GGF100k model (Panovska et al., 2018) and
678 the last 500 kyrs of the ODP Site 983 record (Channell, 1999; Channell et al., 1997). In each of the lower
679 panels, the analysis is performed on the entire GREENICE15k stack (black line) and just the 0-12 ka
680 portion of the GREENICE15k stack (gray stippled line), as the ~12-15 ka portion is only constrained by
681 one core, MD99-2264.

682

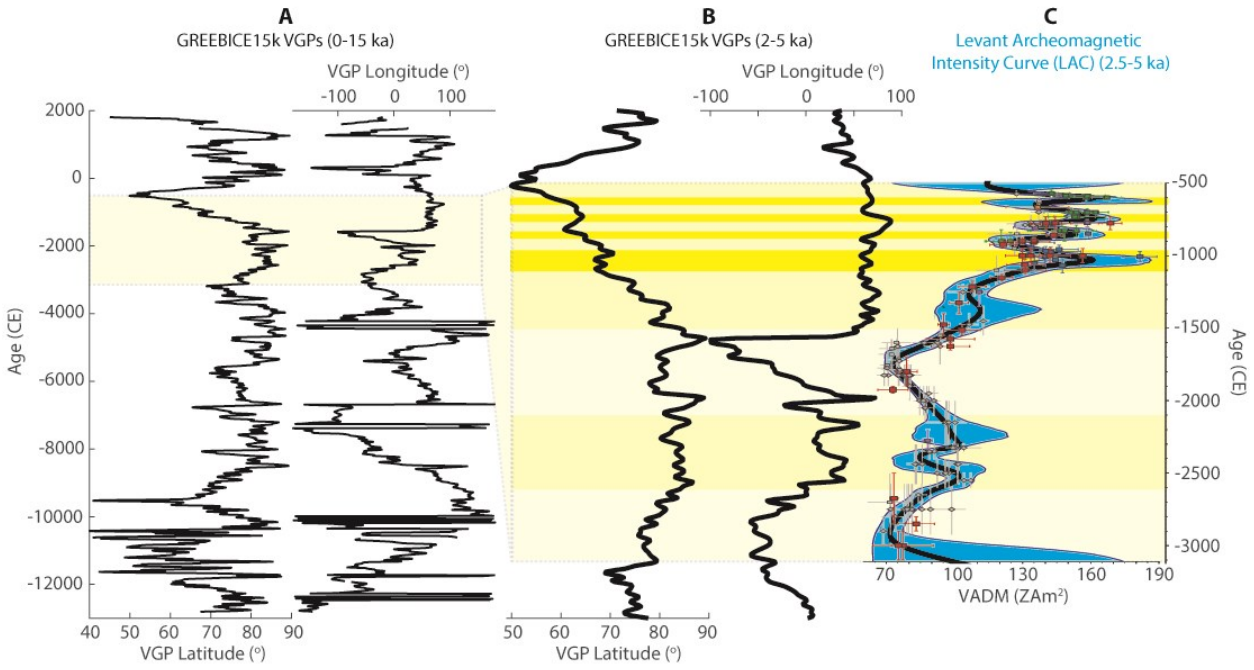

683

684 **Figure 10. Comparison of GREENICE15k to high resolution archeomagnetic intensity data.** Virtual
685 Geomagnetic Pole (VGP) latitudes and longitudes of the GREENICE15k stack (black) for **(A)** the last 15 kyr
686 (left) and **(B)** a zoom in (center) where the stack overlaps with **(C)** the recent 3000 – 500 BCE Levant
687 Archeomagnetic Intenity Curve (LAC) compilation of Shaar et al. (2022; blue shading and points on
688 right). Yellow shading is used to highlight the time interval of comparison and intervals of high
689 paleointensity in the Levant region.

References

Anderson, D.M., 2001. Attenuation of millennial-scale events by bioturbation in marine sediments. Paleoceanography 16, 352–357. https://doi.org/10.1029/2000PA000530

Andrews, J.T., Hardadottir, J., Stoner, J.S., Mann, M.E., Kristjansdottir, G.B., Koc, N., 2003. Decadal to millennial-scale periodicities in North Iceland shelf sediments over the last 12 000 cal yr: long-term North Atlantic oceanographic variability and solar forcing. Earth and Planetary Science Letters 210, 453–465. https://doi.org/10.1016/S0012-821X(03)00139-0

Andrews, J.T., Hardardóttir, J., Stoner, J.S., Principato, S.M., 2008. Holocene Sediment Magnetic Properties along a Transect From Ísafjardardjúp to Djúpáll, Northwest Iceland. Arctic, Antarctic, and Alpine Research 40, 1–14. https://doi.org/10.1657/1523-0430(05-072)[ANDREWS]2.0.CO;2

Balbas, A.M., Koppers, A.A.P., Clark, P.U., Coe, R.S., Reilly, B.T., Stoner, J.S., Konrad, K., 2018. Millennial-Scale Instability in the Geomagnetic Field Prior to the Matuyama-Brunhes Reversal. Geochemistry, Geophysics, Geosystems 19, 952–967. https://doi.org/10.1002/2017GC007404

Ballini M., Kissel C., Colin C., & Richter T. (2006). Deep-water mass source and dynamic associated with rapid climatic variations during the last glacial stage in the North Atlantic: A multiproxy investigation of the detrital fraction of deep-sea sediments. Geochemistry, Geophysics, Geosystems, 7(2). https://doi.org/10.1029/2005GC001070

Bondevik, S., Mangerud, J., Birks, H.H., Gulliksen, S., Reimer, P., 2006. Changes in North Atlantic Radiocarbon Reservoir Ages During the Allerød and Younger Dryas. Science 312, 1514–1517. https://doi.org/10.1126/science.1123300

Bowles, J., 2009. SQUID Attack. The IRM Quarterly 19(1), 1-11.

Cabedo-Sanz, P., Belt, S.T., Jennings, A.E., Andrews, J.T., Geirsdóttir, Á., 2016. Variability in drift ice export from the Arctic Ocean to the North Icelandic Shelf over the last 8000 years: A multi-proxy evaluation. Quaternary Science Reviews 146, 99–115. https://doi.org/10.1016/j.quascirev.2016.06.012

Cao, L., Fairbanks, R.G., Mortlock, R.A., Risk, M.J., 2007. Radiocarbon reservoir age of high latitude North Atlantic surface water during the last deglacial. Quaternary Science Reviews 26, 732–742. https://doi.org/10.1016/j.quascirev.2006.10.001

Caron, M., St-Onge, G., Montero-Serrano, J.-C., Rochon, A., Georgiadis, E., Giraudeau, J., Massé, G., 2019. Holocene chronostratigraphy of northeastern Baffin Bay based on radiocarbon and palaeomagnetic data. Boreas 48, 147–165. https://doi.org/10.1111/bor.12346

721 Channell, J.E.T., 1999. Geomagnetic paleointensity and directional secular variation at Ocean Drilling
722 Program (ODP) Site 984 (Bjorn Drift) since 500 ka: Comparisons with ODP Site 983 (Gardar Drift).
723 J. Geophys. Res. 104, 22937–22951. https://doi.org/10.1029/1999JB900223
724 Channell, J.E.T., Guyodo, Y., 2004. The Matuyama Chronozone at ODP Site 982 (Rockall Bank): Evidence
725 for Decimeter-Scale Magnetization Lock-In Depths, in: Channell, J.E.T., Kent, D.V., Lowrie, W.,
726 Meert, J.G. (Eds.), Timescales Of The Paleomagnetic Field. American Geophysical Union, pp.
727 205–219.
728 Channell, J.E.T., Hodell, D.A., Lehman, B., 1997. Relative geomagnetic paleointensity and δ18O at ODP
729 Site 983 (Gardar Drift, North Atlantic) since 350 ka. Earth and Planetary Science Letters 153,
730 103–118. https://doi.org/10.1016/S0012-821X(97)00164-7
731 Channell, J.E.T., Xuan, C., Hodell, D.A., 2009. Stacking paleointensity and oxygen isotope data for the last
732 1.5 Myr (PISO-1500). Earth and Planetary Science Letters 283, 14–23.
733 Constable, C., Korte, M., Panovska, S., 2016. Persistent high paleosecular variation activity in southern
734 hemisphere for at least 10 000 years. Earth and Planetary Science Letters 453, 78–86.
735 https://doi.org/10.1016/j.epsl.2016.08.015
736 Day, R., Fuller, M., & Schmidt, V. (1977). Hysteresis properties of titanomagnetites, grain size and
737 compositional dependence. Physics of the Earth and Planetary Interiors, 13(4), 260–267.
738 Eiríksson, J., Larsen, G., Knudsen, K.L., Heinemeier, J., Símonarson, L.A., 2004. Marine reservoir age
739 variability and water mass distribution in the Iceland Sea. Quaternary Science Reviews, Holocene
740 climate variability - a marine perspective 23, 2247–2268.
741 https://doi.org/10.1016/j.quascirev.2004.08.002
742 Evans, H. F., Channell, J. E. T., Stoner, J. S., Hillaire-Marcel, C., Wright, J. D., Neitzke, L. C., & Mountain, G.
743 S. (2007). Paleointensity-assisted chronostratigraphy of detrital layers on the Eirik Drift (North
744 Atlantic) since marine isotope stage 11. Geochemistry, Geophysics, Geosystems, 8(11).
745 https://doi.org/10.1029/2007GC001720
746 Geirsdóttir, Á., Andrews, J.T., Ólafsdóttir, S., Helgadóttir, G., Hardardóttir, J., 2002. A 36 Ky record of
747 iceberg rafting and sedimentation from north-west Iceland. Polar Research 21, 291–298.
748 Geirsdóttir, Á., Harning, D.J., Miller, G.H., Andrews, J.T., Zhong, Y., Caseldine, C., 2020. Holocene history
749 of landscape instability in Iceland: Can we deconvolve the impacts of climate, volcanism and
750 human activity? Quaternary Science Reviews 249, 106633.
751 https://doi.org/10.1016/j.quascirev.2020.106633

752 Gudmundsdóttir, E.R., Eiríksson, J., Larsen, G., 2011. Identification and definition of primary and
753 reworked tephra in Late Glacial and Holocene marine shelf sediments off North Iceland. Journal
754 of Quaternary Science 26, 589–602. https://doi.org/10.1002/jqs.1474
755 Hagen, C.J., Reilly, B.T., Stoner, J.S., Creveling, J.R., 2020. Dynamic time warping of palaeomagnetic
756 secular variation data. Geophys J Int 221, 706–721. https://doi.org/10.1093/gji/ggaa004
757 Haltia-Hovi, E., Nowaczyk, N., Saarinen, T., 2010. Holocene palaeomagnetic secular variation recorded in
758 multiple lake sediment cores from eastern Finland. Geophys. J. Int. 180, 609–622.
759 https://doi.org/10.1111/j.1365-246X.2009.04456.x
760 Harning, D., Thordarson, T., Geirsdóttir, Á., Miller, G., Florian, C., 2022. Multiple Early Holocene
761 eruptions of Katla produced tephra layers with similar composition to the Vedde Ash.
762 Geochronology Discussions 1–16. https://doi.org/10.5194/gchron-2022-26
763 Hatfield, R. G., Stoner, J. S., Carlson, A. E., Reyes, A. V., & Housen, B. A. (2013). Source as a controlling
764 factor on the quality and interpretation of sediment magnetic records from the northern North
765 Atlantic. Earth and Planetary Science Letters, 368, 69–77.
766 https://doi.org/10.1016/j.epsl.2013.03.001
767 Hatfield, R. G., Stoner, J. S., Reilly, B. T., Tepley, F. J., Wheeler, B. H., & Housen, B. A. (2017). Grain size
768 dependent magnetic discrimination of Iceland and South Greenland terrestrial sediments in the
769 northern North Atlantic sediment record. Earth and Planetary Science Letters, 474, 474–489.
770 https://doi.org/10.1016/j.epsl.2017.06.042
771 Hatfield, R.G., Wheeler, B.H., Reilly, B.T., Stoner, J.S., Housen, B.A., 2019. Particle Size Specific Magnetic
772 Properties Across the Norwegian-Greenland Seas: Insights Into the Influence of Sediment Source
773 and Texture on Bulk Magnetic Records. Geochemistry, Geophysics, Geosystems 20.
774 https://doi.org/10.1029/2018GC007894
775 Hay, C.C., Creveling, J.R., Hagen, C.J., Maloof, A.C., Huybers, P., 2019. A library of early Cambrian
776 chemostratigraphic correlations from a reproducible algorithm. Geology 47, 457–460.
777 https://doi.org/10.1130/G46019.1
778 Heaton, T.J., Bard, E., Bronk Ramsey, C., Butzin, M., Hatté, C., Hughen, K.A., Köhler, P., Reimer, P.J.,
779 2022. A RESPONSE TO COMMUNITY QUESTIONS ON THE MARINE20 RADIOCARBON AGE
780 CALIBRATION CURVE: MARINE RESERVOIR AGES AND THE CALIBRATION OF ^{14}C SAMPLES FROM
781 THE OCEANS. Radiocarbon 1–27. https://doi.org/10.1017/RDC.2022.66
782 Heaton, T.J., Köhler, P., Butzin, M., Bard, E., Reimer, R.W., Austin, W.E.N., Ramsey, C.B., Grootes, P.M.,
783 Hughen, K.A., Kromer, B., Reimer, P.J., Adkins, J., Burke, A., Cook, M.S., Olsen, J., Skinner, L.C.,

2020. Marine20—The Marine Radiocarbon Age Calibration Curve (0–55,000 cal BP). Radiocarbon 62, 779–820. https://doi.org/10.1017/RDC.2020.68

Husson, D., Thibault, N., Galbrun, B., Gardin, S., Minoletti, F., Sageman, B., Huret, E., 2014. Lower Maastrichtian cyclostratigraphy of the Bidart section (Basque Country, SW France): A remarkable record of precessional forcing. Palaeogeography, Palaeoclimatology, Palaeoecology 395, 176–197. https://doi.org/10.1016/j.palaeo.2013.12.008

Jackson, A., Jonkers, A.R., Walker, M.R., 2000. Four centuries of geomagnetic secular variation from historical records. Philosophical Transactions of the Royal Society of London A: Mathematical, Physical and Engineering Sciences 358, 957–990.

Jennings, A., Thordarson, T., Zalzal, K., Stoner, J., Hayward, C., Geirsdóttir, Á., Miller, G., 2014. Holocene tephra from Iceland and Alaska in SE Greenland Shelf Sediments. Geological Society, London, Special Publications 398, SP398.6. https://doi.org/10.1144/SP398.6

Jennings, A.E., Grönvold, K., Hilberman, R., Smith, M., Hald, M., 2002. High-resolution study of Icelandic tephras in the Kangerlussuaq Trough, southeast Greenland, during the last deglaciation. Journal of Quaternary Science 17, 747–757. https://doi.org/10.1002/jqs.692

Jennings, A.E., Hald, M., Smith, M., Andrews, J.T., 2006. Freshwater forcing from the Greenland Ice Sheet during the Younger Dryas: evidence from southeastern Greenland shelf cores. Quaternary Science Reviews 25, 282–298. https://doi.org/10.1016/j.quascirev.2005.04.006

King, J., Peck, J., 2002. Use of Paleomagnetism in Studies of Lake Sediments, in: Last, W.M., Smol, J.P. (Eds.), Tracking Environmental Change Using Lake Sediments, Developments in Paleoenvironmental Research. Springer Netherlands, pp. 371–389. https://doi.org/10.1007/0-306-47669-X_14

Kirschvink, J.L., 1980. The least-squares line and plane and the analysis of palaeomagnetic data. Geophysical Journal of the Royal Astronomical Society 62, 699–718.

Kissel, C., Laj, C., Labeyrie, L., Dokken, T., Voelker, A., & Blamart, D. (1999). Rapid climatic variations during marine isotopic stage 3: magnetic analysis of sediments from Nordic Seas and North Atlantic. Earth and Planetary Science Letters, 171(3), 489–502. https://doi.org/10.1016/S0012-821X(99)00162-4

Kissel, C., Laj, C., Mulder, T., Wandres, C., & Cremer, M. (2009). The magnetic fraction: A tracer of deep water circulation in the North Atlantic. Earth and Planetary Science Letters, 288(3), 444–454. https://doi.org/10.1016/j.epsl.2009.10.005

Korte, M., Brown, M.C., Gunnarson, S.R., Nilsson, A., Panovska, S., Wardinski, I., Constable, C.G., 2019. Refining Holocene geochronologies using palaeomagnetic records. Quaternary Geochronology 50, 47–74. https://doi.org/10.1016/j.quageo.2018.11.004

Kristjánsdóttir, G.B., Moros, M., Andrews, J.T., Jennings, A.E., 2017. Holocene Mg/Ca, alkenones, and light stable isotope measurements on the outer North Iceland shelf (MD99-2269): A comparison with other multi-proxy data and sub-division of the Holocene. The Holocene 27, 52–62. https://doi.org/10.1177/0959683616652703

Kristjánsdóttir, G.B., Stoner, J.S., Jennings, A.E., Andrews, J.T., Grönvold, K., 2007. Geochemistry of Holocene cryptotephras from the North Iceland Shelf (MD99-2269): intercalibration with radiocarbon and palaeomagnetic chronostratigraphies. The Holocene 17, 155–176. https://doi.org/10.1177/0959683607075829

Lisiecki, L.E., Raymo, M.E., 2005. A Pliocene-Pleistocene stack of 57 globally distributed benthic $\delta^{18}O$ records. Paleoceanography 20, PA1003. https://doi.org/10.1029/2004PA001071

Lougheed, B., Obrochta, S., 2019. A Rapid, Deterministic Age-Depth Modeling Routine for Geological Sequences With Inherent Depth Uncertainty. Paleoceanography and Paleoclimatology 0. https://doi.org/10.1029/2018PA003457

Lougheed, B.C., Nilsson, A., Björck, S., Snowball, I., Muscheler, R., 2014. A deglacial palaeomagnetic master curve for Fennoscandia – Providing a dating template and supporting millennial-scale geomagnetic field patterns for the past 14 ka. Quaternary Science Reviews, Dating, Synthesis, and Interpretation of Palaeoclimatic Records and Model-data Integration: Advances of the INTIMATE project(INTegration of Ice core, Marine and TErrestrial records, COST Action ES0907) 106, 155–166. https://doi.org/10.1016/j.quascirev.2014.03.008

Lund, S.P., Keigwin, L., 1994. Measurement of the degree of smoothing in sediment paleomagnetic secular variation records: an example from late Quaternary deep-sea sediments of the Bermuda Rise, western North Atlantic Ocean. Earth and Planetary Science Letters 122, 317–330. https://doi.org/10.1016/0012-821X(94)90005-1

Nilsson, A., Suttie, N., Stoner, J.S., Muscheler, R., 2022. Recurrent ancient geomagnetic field anomalies shed light on future evolution of the South Atlantic Anomaly. Proceedings of the National Academy of Sciences 119, e2200749119. https://doi.org/10.1073/pnas.2200749119

Nowaczyk, N.R., Arz, H.W., Frank, U., Kind, J., Plessen, B., 2012. Dynamics of the Laschamp geomagnetic excursion from Black Sea sediments. Earth and Planetary Science Letters 351–352, 54–69. https://doi.org/10.1016/j.epsl.2012.06.050

Nowaczyk, N. R., Liu, J., & Arz, H. W. (2021). Records of the Laschamps geomagnetic polarity excursion from Black Sea sediments: magnetite versus greigite, discrete sample versus U-channel data. Geophysical Journal International, 224(2), 1079–1095. https://doi.org/10.1093/gji/ggaa506 https://doi.org/10.1093/gji/ggaa506

Oda, H., & Shibuya, H. (1996). Deconvolution of long-core paleomagnetic data of Ocean Drilling Program by Akaike's Bayesian Information Criterion minimization. Journal of Geophysical Research: Solid Earth, 101(B2), 2815–2834. https://doi.org/10.1029/95JB02811

Óladóttir, B.A., Thordarson, T., Geirsdóttir, Á., Jóhannsdóttir, G.E., Mangerud, J., 2020. The Saksunarvatn Ash and the G10ka series tephra. Review and current state of knowledge. Quaternary Geochronology 56, 101041. https://doi.org/10.1016/j.quageo.2019.101041

Ólafsdóttir, S., 2010. Holocene marine and lacustrine paleoclimate and paleomagnetic records from Iceland: Land-sea correlations (PhD Thesis). University of Iceland, Reykjavik, Iceland.

Ólafsdóttir, S., Geirsdottir, A., Miller, G.H., Stoner, J.S., Channell, J.E.T., 2013. Synchronizing Holocene lacustrine and marine sediment records using paleomagnetic secular variation. Geology 41, 535–538. https://doi.org/10.1130/G33946.1

Ólafsdóttir, S., Jennings, A.E., Geirsdóttir, Á., Andrews, J., Miller, G.H., 2010. Holocene variability of the North Atlantic Irminger current on the south- and northwest shelf of Iceland. Marine Micropaleontology 77, 101–118. https://doi.org/10.1016/j.marmicro.2010.08.002

Ólafsdóttir, S., Reilly, B.T., Bakke, J., Stoner, J.S., Gjerde, M., van der Bilt, W.G.M., 2019. Holocene paleomagnetic secular variation (PSV) near 80° N, Northwest Spitsbergen, Svalbard: Implications for evaluating High Arctic sediment chronologies. Quaternary Science Reviews 210, 90–102. https://doi.org/10.1016/j.quascirev.2019.03.003

Panovska, S., Constable, C.G., Korte, M., 2018. Extending global continuous geomagnetic field reconstructions on timescales beyond human civilization. Geochemistry, Geophysics, Geosystems. https://doi.org/10.1029/2018GC007966

Panovska, S., Korte, M., Constable, C.G., 2019. One Hundred Thousand Years of Geomagnetic Field Evolution. Reviews of Geophysics n/a. https://doi.org/10.1029/2019RG000656

Panovska, S., Korte, M., Liu, J., Nowaczyk, N., 2021. Global Evolution and Dynamics of the Geomagnetic Field in the 15–70 kyr Period Based on Selected Paleomagnetic Sediment Records. Journal of Geophysical Research: Solid Earth 126, e2021JB022681. https://doi.org/10.1029/2021JB022681

877 Pavón-Carrasco, F.J., Osete, M.L., Torta, J.M., De Santis, A., 2014. A geomagnetic field model for the
878 Holocene based on archaeomagnetic and lava flow data. Earth and Planetary Science Letters
879 388, 98–109. https://doi.org/10.1016/j.epsl.2013.11.046
880 Peck, J.A., King, J.W., Colman, S.M., Kravchinsky, V.A., 1996. An 84-kyr paleomagnetic record from the
881 sediments of Lake Baikal, Siberia. J. Geophys. Res. 101, 11365–11385.
882 https://doi.org/10.1029/96JB00328
883 Quillmann, U., Jennings, A., Andrews, J., 2010. Reconstructing Holocene palaeoclimate and
884 palaeoceanography in Ìsafjarðardjúp, northwest Iceland, from two fjord records overprinted by
885 relative sea-level and local hydrographic changes. Journal of Quaternary Science 25, 1144–1159.
886 https://doi.org/10.1002/jqs.1395
887 Reilly, B.T., Stoner, J.S., Hatfield, R.G., Abbott, M.B., Marchetti, D.W., Larsen, D.J., Finkenbinder, M.S.,
888 Hillman, A.L., Kuehn, S.C., Heil, C.W., 2018. Regionally consistent Western North America
889 paleomagnetic directions from 15 to 35 ka: Assessing chronology and uncertainty with
890 paleosecular variation (PSV) stratigraphy. Quaternary Science Reviews 201, 186–205.
891 https://doi.org/10.1016/j.quascirev.2018.10.016
892 Reilly, B.T., Stoner, J.S., Mix, A.C., Walczak, M.H., Jennings, A., Jakobsson, M., Dyke, L., Glueder, A.,
893 Nicholls, K., Hogan, K.A., Mayer, L.A., Hatfield, R.G., Albert, S., Marcott, S., Fallon, S., Cheseby,
894 M., 2019. Holocene break-up and reestablishment of the Petermann Ice Tongue, Northwest
895 Greenland. Quaternary Science Reviews 218, 322–342.
896 https://doi.org/10.1016/j.quascirev.2019.06.023
897 Reimer, P.J., Bard, E., Bayliss, A., Beck, J.W., Blackwell, P.G., Ramsey, C.B., Buck, C.E., Cheng, H., Edwards,
898 R.L., Friedrich, M., Grootes, P.M., Guilderson, T.P., Haflidason, H., Hajdas, I., Hatté, C., Heaton,
899 T.J., Hoffmann, D.L., Hogg, A.G., Hughen, K.A., Kaiser, K.F., Kromer, B., Manning, S.W., Niu, M.,
900 Reimer, R.W., Richards, D.A., Scott, E.M., Southon, J.R., Staff, R.A., Turney, C.S.M., Plicht, J. van
901 der, 2013. IntCal13 and Marine13 Radiocarbon Age Calibration Curves 0–50,000 Years cal BP.
902 Radiocarbon 55, 1869–1887. https://doi.org/10.2458/azu_js_rc.55.16947
903 Roberts, A.P., Winklhofer, M., 2004. Why are geomagnetic excursions not always recorded in
904 sediments? Constraints from post-depositional remanent magnetization lock-in modelling. Earth
905 and Planetary Science Letters 227, 345–359. https://doi.org/10.1016/j.epsl.2004.07.040
906 Ryan, W. B. F., Carbotte, S. M., Coplan, J. O., O'Hara, S., Melkonian, A., Arko, R., et al. (2009). Global
907 Multi-Resolution Topography synthesis. Geochemistry, Geophysics, Geosystems, 10(3).
908 https://doi.org/10.1029/2008GC002332

Sadhasivan, M., Constable, C., 2022. A new power spectrum and stochastic representation for the geomagnetic axial dipole. Geophysical Journal International 231, 15–26. https://doi.org/10.1093/gji/ggac172

Shaar, R., Gallet, Y., Vaknin, Y., Gonen, L., Martin, M.A.S., Adams, M.J., Finkelstein, I., 2022. Archaeomagnetism in the Levant and Mesopotamia Reveals the Largest Changes in the Geomagnetic Field. Journal of Geophysical Research: Solid Earth 127, e2022JB024962. https://doi.org/10.1029/2022JB024962

Simon, Q., Bourlès, D.L., Thouveny, N., Horng, C.-S., Valet, J.-P., Bassinot, F., Choy, S., 2018. Cosmogenic signature of geomagnetic reversals and excursions from the Réunion event to the Matuyama–Brunhes transition (0.7–2.14 Ma interval). Earth and Planetary Science Letters 482, 510–524. https://doi.org/10.1016/j.epsl.2017.11.021

Snowball, I. F., & Moros, M. (2003). Saw-tooth pattern of North Atlantic current speed during Dansgaard-Oeschger cycles revealed by the magnetic grain size of Reykjanes Ridge sediments at 59°N. Paleoceanography, 18(2). https://doi.org/10.1029/2001PA000732

Stern, J.V., Lisiecki, L.E., 2013. North Atlantic circulation and reservoir age changes over the past 41,000 years. Geophysical Research Letters 40, 3693–3697. https://doi.org/10.1002/grl.50679

Stockhausen, H., 1998. Geomagnetic palaeosecular variation (0–13 000 yr BP) as recorded in sediments from three maar lakes from the West Eifel (Germany). Geophys J Int 135, 898–910. https://doi.org/10.1046/j.1365-246X.1998.00664.x

Stoner, J.S., Channell, J.E.T., Mazaud, A., Strano, S.E., Xuan, C., 2013. The influence of high-latitude flux lobes on the Holocene paleomagnetic record of IODP Site U1305 and the northern North Atlantic. Geochemistry, Geophysics, Geosystems 14, 4623–4646. https://doi.org/10.1002/ggge.20272

Stoner, J.S., Jennings, A., Kristjánsdóttir, G.B., Dunhill, G., Andrews, J.T., Hardardóttir, J., 2007. A paleomagnetic approach toward refining Holocene radiocarbon-based chronologies: Paleoceanographic records from the north Iceland (MD99-2269) and east Greenland (MD99-2322) margins. Paleoceanography 22. https://doi.org/10.1029/2006PA001285

Strunk, A., Larsen, N.K., Nilsson, A., Seidenkrantz, M.-S., Levy, L.B., Olsen, J., Lauridsen, T.L., 2018. Relative sea-level changes and ice sheet history in Finderup Land, North Greenland. Frontiers in Earth Science 6, 129.

Stuiver, M., Pearson, G.W., Braziunas, T., 1986. Radiocarbon age calibration of marine samples back to 9000 cal yr BP. Radiocarbon 28, 980–1021.

941 Suganuma, Y., Yokoyama, Y., Yamazaki, T., Kawamura, K., Horng, C.-S., Matsuzaki, H., 2010. 10Be
942 evidence for delayed acquisition of remanent magnetization in marine sediments: Implication
943 for a new age for the Matuyama–Brunhes boundary. Earth and Planetary Science Letters 296,
944 443–450. https://doi.org/10.1016/j.epsl.2010.05.031
945 Tauxe, L., Herbert, T., Shackleton, N.J., Kok, Y.S., 1996. Astronomical calibration of the Matuyama-
946 Brunhes boundary: Consequences for magnetic remanence acquisition in marine carbonates
947 and the Asian loess sequences. Earth and Planetary Science Letters 140, 133–146.
948 Thompson, R., 1984. A global review of paleomagnetic results from wet lake sediments, in: Haworth,
949 E.Y., Lund, J.W.G. (Eds.), Lake Sediments and Environmental History: Studies in Palaeolimnology
950 and Palaeoecology in Honour of Winifred Tutin. University of Minnesota Press, Minneapolis, pp.
951 145–164.
952 Walczak, M.H., Stoner, J.S., Mix, A.C., Jaeger, J., Rosen, G.P., Channell, J.E.T., Heslop, D., Xuan, C., 2017.
953 A 17,000 yr paleomagnetic secular variation record from the southeast Alaskan margin: Regional
954 and global correlations. Earth and Planetary Science Letters 473, 177–189.
955 https://doi.org/10.1016/j.epsl.2017.05.022
956 Wanamaker, A.D., Butler, P.G., Scourse, J.D., Heinemeier, J., Eiríksson, J., Knudsen, K.L., Richardson, C.A.,
957 2012. Surface changes in the North Atlantic meridional overturning circulation during the last
958 millennium. Nature Communications 3, 899. https://doi.org/10.1038/ncomms1901
959 Wang, H., Kent, D.V., Rochette, P., 2015. Weaker axially dipolar time-averaged paleomagnetic field
960 based on multidomain-corrected paleointensities from Galapagos lavas. PNAS 112, 15036–
961 15041. https://doi.org/10.1073/pnas.1505450112
962 Xuan, C., Channell, J.E.T., 2009. UPmag: MATLAB software for viewing and processing u channel or other
963 pass-through paleomagnetic data. Geochemistry, Geophysics, Geosystems 10.
964 https://doi.org/10.1029/2009GC002584
965 Xuan, C., Oda, H., 2015. UDECON: deconvolution optimization software for restoring high-resolution
966 records from pass-through paleomagnetic measurements. Earth Planet Sp 67, 1–17.
967 https://doi.org/10.1186/s40623-015-0332-x
968
969
970